Physica A 524 (2019) 130–146

Contents lists available at ScienceDirect

Physica A

journal homepage: www.elsevier.com/locate/physa

Partially polarized black-body radiation

Roman Tomaschitz

Sechsschimmelgasse 1/21-22, A-1090 Vienna, Austria

HIGHLIGHTS

- Black-body radiation can be fractionally polarized due to angular-dependent temperature fluctuations.
- The spectral density of a partially polarized photon gas is derived and related to the Stokes parameters.
- Spatial energy density correlations induced by temperature and polarization anisotropy are derived.
- Analytic Gaussian representations of polarization power spectra are obtained via least-squares fits.
- Long-range correlations of the microwave background radiation are calculated from angular power spectra.

ARTICLE INFO

Article history:
Received 19 July 2018
Received in revised form 19 September 2018
Available online 14 March 2019

Keywords:
Polarized photon gas
Polarization fraction
Stokes parameters of anisotropic black-body radiation
Multipole expansion of angular fluctuations
Spatial energy density correlations
Cosmic microwave background radiation

ABSTRACT

Angular temperature fluctuations in a photon gas generate fractional polarization of the black-body spectrum. The spectral density consists of two Planckians with different temperature variables representing orthogonal polarization states. The angular-dependent fluctuating temperature variables can be inferred from the Stokes parameters which have been measured, over the full solid angle, for the cosmic microwave background (CMB) radiation. The polarization matrix of a partially polarized photon gas is obtained by way of a unitary transformation of the annihilation and creation operators. The radiation is decomposed into a totally polarized and an unpolarized intensity component, and the polarization fraction is calculated, which is very small, of order $\sim 10^{-7}$, for the nearly isotropic CMB radiation. Spatial energy density autocorrelations induced by polarization and temperature anisotropy are derived and isotropized by an angular average. These correlations are long-range, exhibiting power-law decay $\propto 1/r^6$ at large distance, and much stronger than the energy density correlation of an ideal photon gas which decays $\propto 1/r^8$. As for the CMB radiation, the spatial energy density correlations are calculated from analytic Gaussian fits to the measured temperature and polarization power spectra, including the crossover from the short-distance regime to the asymptotic power-law decay.

1. Introduction

We study fractional polarization of the black-body spectrum, caused by angular temperature fluctuations, which has been measured with high precision in the case of the cosmic microwave background (CMB) radiation [1–3]. The ideal photon gas as described by the Planck distribution amounts to totally unpolarized radiation. The spectral density of partially polarized black-body radiation consists of two Planckians with independent temperature variables, one for each polarization degree of freedom. The angular variation of the temperature variables can be determined by measuring the Stokes parameters.

E-mail address: tom@geminga.org.

https://doi.org/10.1016/j.physa.2019.03.014
0378-4371/

We derive the spectral density of a partially polarized photon gas, starting with the statistical operator, reconstruct the operator of the electric field strength from the Stokes parameters and assemble the polarization matrix. We then study the effect of polarization and angular anisotropy on two-point and four-point correlation functions of the electric field strength, in particular on spatial energy density autocorrelations generated by temperature anisotropy and fractional polarization. We expand the correlation functions in the fluctuating temperature variables and isotropize them by performing an angular average.

The CMB radiation will be used as example throughout this paper, since the angular temperature and polarization fluctuations have been measured over the full solid angle and are very small, which makes an efficient perturbative treatment of the energy density correlations possible, including the extended crossover from the short- to the long-distance regime. The energy density correlations of a fractionally polarized photon gas are long-range, nearly constant at short distance and exhibiting power-law decay in the opposite limit.

Long-range correlations have extensively been applied to characterize phase transitions [4–7] and fracture statistics [8], and they also occur frequently in plasma and nuclear physics [9,10], as well as in interdisciplinary fields such as meteorology and geophysics [11–13], biophysics [14,15], econophysics [16,17], sociophysics [18], human dynamics [19] and network theory [20,21].

In Section 2, we introduce the statistical operator of an anisotropic and polarized photon gas and derive the partition function and spectral density, the latter being a superposition of two Planckians with temperature variables depending on the photonic wave vector, as well as the entropy. We also sketch the variances and the factorization of expectation values of operator products in the thermodynamic limit, used employed in Section 4 to calculate energy density correlations.

In Section 3, we introduce the operators defining the polarized electric field strengths and calculate the expectation values of their products constituting the polarization matrix. The phases and amplitudes of the field strengths and in particular the fluctuating temperature variables of the spectral densities can be inferred from the angular-dependent Stokes parameters. We perform a second-order expansion of the spectral densities in the angular fluctuations around the mean temperature and decompose the spectral intensity into a totally polarized and an unpolarized radiation component.

In Section 4, we study spatial correlation functions. First, we calculate the two-point correlation of the electric field strength, relating it to the two Planckians defining the spectral density. Then we derive the energy density autocorrelation of an anisotropic and partially polarized photon gas, which is a four-point correlation of the electric field strength.

In Section 5, we perform angular fluctuation averages to isotropize the spectral intensities and spatial correlation functions. To this end, we use multipole expansions of the temperature and polarization correlations in momentum space. The multipole coefficients of the CMB radiation have been measured up to multipole indices of $l \sim 2500$, cf. Ref. [3]. In Section 5.2, we obtain analytic representations of the power spectra of the temperature and polarization autocorrelations and their cross-correlation by performing spectral fits with a series of Gaussians.

In Section 5.3, we isotropize the polarized and unpolarized intensity components of a photon gas by a fluctuation average. In particular, we estimate the polarized and unpolarized spectral intensities of the CMB radiation from the Gaussian fits to the multipole power spectra. We calculate the specific internal energy of these components to obtain the polarization fraction, which is very small in the case of the CMB radiation; only a 2.4×10^{-7} fraction of the internal energy is polarized. Presently, only the Stokes parameters Q and U defining linear polarization have been measured. In Section 5.4, we isotropize the energy density correlations induced by angular temperature and polarization fluctuations, using the above mentioned multipole expansions.

The fluctuation-induced energy density correlations are long-range, $\propto 1/r^6$, and overpower the isotropic correlation function of an ideal photon gas, which decays $\propto 1/r^8$ in the large-distance limit. This is illustrated by plots of the CMB correlations in Section 6; the fluctuation-induced correlations stay nearly constant in the short-distance regime up to about $r\sim 0.01$ cm and admit power-law decay $\propto 1/r^6$ following an extended crossover covering four decades in distance. In Section 7, we present our conclusions.

2. Spectral density of an anisotropic and partially polarized photon gas

2.1. Statistical operator, partition function and expectation values

We start with a discrete mode decomposition of the electromagnetic field strength,

$$\mathbf{E}(\mathbf{x},t)=\frac{1}{\sqrt{2L^3}}\sum_{\mathbf{k}}(\mathbf{E}_{\mathbf{k}}\mathrm{e}^{\mathrm{i}(\mathbf{kx}-\omega t)}+\mathbf{E}^*_{\mathbf{k}}\mathrm{e}^{-\mathrm{i}(\mathbf{kx}-\omega t)}), \tag{2.1}$$

with $\omega=|\mathbf{k}|$, and use box quantization, discretizing the wave vector as $\mathbf{k}=2\pi\mathbf{n}/L$, $\mathbf{n}\in Z^3$, where L is the box size. The magnetic field $\mathbf{B}(\mathbf{x},t)$ admits an analogous expansion with $\mathbf{B}_{\mathbf{k}}=\mathbf{k}_0\times\mathbf{E}_{\mathbf{k}}$, where $\mathbf{k}_0$ is the unit wave vector. We split the amplitudes into polarization components, $\mathbf{E}_{\mathbf{k}}=\boldsymbol{\varepsilon}_1E_{1,\mathbf{k}}+\boldsymbol{\varepsilon}_2E_{2,\mathbf{k}}$, where the polarization vectors $\boldsymbol{\varepsilon}_{j=1,2}$ and $\mathbf{k}_0$ constitute an orthonormal triad. By squaring the field strength and performing a time average, we find the energy density

$$\mathbf{E}^2(\mathbf{x},t)=\mathbf{B}^2(\mathbf{x},t)=\frac{1}{L^3}\sum_{j,\mathbf{k}}E^*_{j,\mathbf{k}}E_{j,\mathbf{k}}. \tag{2.2}$$

We symmetrize the product $E^*_{j,\mathbf{k}}E_{j,\mathbf{k}}$ and replace the field modes by bosonic annihilation and creation operators $a_{j,\mathbf{k}}$ and $a^\dagger_{j,\mathbf{k}}$, identifying $E_{j,\mathbf{k}} = \sqrt{\omega_{j,\mathbf{k}}}a_{j,\mathbf{k}}$, $E^*_{j,\mathbf{k}} \to E^\dagger_{j,\mathbf{k}} = \sqrt{\omega_{j,\mathbf{k}}}a^\dagger_{j,\mathbf{k}}$, with $\omega_{j,\mathbf{k}} = k$. The $a_{j,\mathbf{k}}$ and their adjoints satisfy the commutation relations $[a_i, a^\dagger_n] = \delta_{in}$, $[a_i, a_n] = 0$ and $[a^\dagger_i, a^\dagger_n] = 0$, where we use a multi-index notation as shortcut, $i = (j, \mathbf{k})$, and $j = 1, 2$ labels the two polarization degrees. Finally, we split the energy operator $H = \int_{L^3} \mathbf{E}^2(\mathbf{x}, t)\mathrm{d}\mathbf{x}$ into polarization components, $H = H_1 + H_2$, $H_j = \sum_{\mathbf{k}} H_{j,\mathbf{k}}$,

$$H_{j,\mathbf{k}} = \frac{1}{2}(E^\dagger_{j,\mathbf{k}}E_{j,\mathbf{k}} + E_{j,\mathbf{k}}E^\dagger_{j,\mathbf{k}}) = \omega_{j,\mathbf{k}}(N_{j,\mathbf{k}} + \frac{1}{2}), \tag{2.3}$$

where the $N_{j,\mathbf{k}} = a^\dagger_{j,\mathbf{k}}a_{j,\mathbf{k}}$ are commuting hermitian particle number operators; $[a_n, N_m] = \delta_{nm}a_n$ and $[a^\dagger_n, N_m] = -\delta_{nm}a^\dagger_n$.

We use the occupation number representation of the a_i and $a^\dagger_i$, with normalized basis vectors $|n_1, \ldots, n_i, \ldots, n_\infty\rangle$ (shortcut $|n\rangle$, e.g. $|0\rangle$ for the vacuum state). The occupation numbers n_i are non-negative integers indicating the number of particles in state i. A scalar product is defined by $\langle n|n'\rangle = \delta_{n_1,n'_1}\ldots\delta_{n_\infty,n'_\infty}$. The representation of the a_i and $a^\dagger_i$ then reads

$$\begin{aligned} a_i|n_1, \ldots, n_i, \ldots, n_\infty\rangle &= \sqrt{n_i}|n_1, \ldots, n_i - 1, \ldots, n_\infty\rangle,\\ a^\dagger_i|n_1, \ldots, n_i, \ldots, n_\infty\rangle &= \sqrt{n_i + 1}|n_1, \ldots, n_i + 1, \ldots, n_\infty\rangle, \end{aligned} \tag{2.4}$$

and $a_i|n\rangle = 0$ (zero-vector) if $n_i = 0$. Hence, $\langle a^\dagger_i n|n'\rangle = \langle n|a_i n'\rangle$. The particle number operators $N_i = a^\dagger_i a_i$ are hermitian, commute, and are diagonal in this representation, $N_i|n\rangle = n_i|n\rangle$.

We define the density operator of an anisotropic polarized photon gas as $\hat\rho = \exp(-H_{\hat T})$, $H_{\hat T} = \sum_{j,\mathbf{k}} H_{j,\mathbf{k}}/\hat T_{j,\mathbf{k}}$, with angular dependent (and possibly also frequency dependent) temperatures $\hat T_{j,\mathbf{k}} = \hat T_j(\omega, \mathbf{k}_0)$ which differ for the polarization states $j = 1, 2$. The partition function is $Z = \mathrm{Tr}[\hat\rho]$, and the total internal energy is obtained as expectation value $U = \langle H\rangle = \langle H_1\rangle + \langle H_2\rangle$, $\langle H_j\rangle = \mathrm{Tr}[H_j\hat\rho]/Z$.

To evaluate the expectation value of an operator of type $G = \sum_{j,\mathbf{k}} g_{j,\mathbf{k}}(N_{j,\mathbf{k}} + 1/2)$, where $g_{j,\mathbf{k}}$ is an arbitrary function of j and $\mathbf{k}$ (and other parameters such as space coordinates), we consider $Z_\varepsilon = \mathrm{Tr}[\hat\rho_\varepsilon]$ with $\hat\rho_\varepsilon = \exp(-H_{\hat T} - \varepsilon G)$. Here, ε is a dimensionless parameter put to zero after differentiation, so that $\langle G\rangle = -(\log Z_\varepsilon)_{,\varepsilon} = \mathrm{Tr}[G\hat\rho]/Z$. By employing the above occupation number representation, $\log Z_\varepsilon$ can easily be evaluated. We use the shortcut

$$F_\varepsilon = H_{\hat T} + \varepsilon G = \sum_{j,\mathbf{k}} f_{j,\mathbf{k}}(N_{j,\mathbf{k}} + \frac{1}{2}), \quad f_{j,\mathbf{k}} = (\frac{\omega_{j,\mathbf{k}}}{\hat T_{j,\mathbf{k}}} + \varepsilon g_{j,\mathbf{k}}), \tag{2.5}$$

and find, in multi-index notation $i = (j, \mathbf{k})$,

$$\begin{aligned} Z_\varepsilon &= \sum_{n_1,\ldots,n_\infty=0}^{\infty} \exp(-\sum_{i=1}^{\infty} f_i(n_i + \frac{1}{2})) = \sum_{n_1,\ldots,n_\infty=0}^{\infty} \prod_{i=1}^{\infty} \exp(-f_i(n_i + \frac{1}{2}))\\ &= \prod_{i=1}^{\infty}\sum_{n_i=0}^{\infty} \mathrm{e}^{-f_i(n_i+1/2)} = \prod_{i=1}^{\infty} \mathrm{e}^{-f_i/2}\sum_{n_i=0}^{\infty}\mathrm{e}^{-f_i n_i} = \prod_{i=1}^{\infty}\frac{\mathrm{e}^{-f_i/2}}{1-\mathrm{e}^{-f_i}}. \end{aligned} \tag{2.6}$$

Thus,

$$\log Z_\varepsilon = \sum_{i=1}^{\infty}\log\frac{\mathrm{e}^{-f_i/2}}{1-\mathrm{e}^{-f_i}} = -\sum_{j,\mathbf{k}}(f_{j,\mathbf{k}}/2 + \log(1-\mathrm{e}^{-f_{j,\mathbf{k}}})), \tag{2.7}$$

and by substituting $f_{j,\mathbf{k}}$ in (2.5),

$$\langle G\rangle = -(\log Z_\varepsilon)_{,\varepsilon} = \sum_{j,\mathbf{k}} g_{j,\mathbf{k}}(\frac{1}{\mathrm{e}^{\omega_{j,\mathbf{k}}/\hat T_{j,\mathbf{k}}} - 1} + \frac{1}{2}). \tag{2.8}$$

The continuum limit is performed by replacing $\sum_{\mathbf{k}} \to (L^3/(2\pi)^3)\int \mathrm{d}\mathbf{k}$,

$$\log Z_\varepsilon = -\frac{L^3}{(2\pi)^3}\sum_{j=1}^{2}\int(\log(1-\mathrm{e}^{-f_{j,\mathbf{k}}}) + \frac{1}{2}f_{j,\mathbf{k}})\mathrm{d}\mathbf{k}, \tag{2.9}$$

$$\langle G\rangle = \frac{L^3}{(2\pi)^3}\sum_{j=1}^{2}\int g_{j,\mathbf{k}}(\frac{1}{\mathrm{e}^{\omega_{j,\mathbf{k}}/\hat T_{j,\mathbf{k}}} - 1} + \frac{1}{2})\mathrm{d}\mathbf{k}. \tag{2.10}$$

The expression in parentheses in (2.10) is just $(1/2)\coth(\omega_{j,\mathbf{k}}/(2\hat T_{j,\mathbf{k}}))$. The fermionic counterpart can be dealt with in like manner, requiring only some sign changes and the removal of the zero-point terms [22,23].

To obtain the total energy $\langle H\rangle$, we put $g_{j,\mathbf{k}} = \omega_{j,\mathbf{k}} = k$ in (2.10). In the following, we will usually drop the infinite vacuum energy generated by the 1/2 term in (2.10). Eq. (2.3) then simplifies to $H_j = \sum_{\mathbf{k}} H_{j,\mathbf{k}}$ with $H_{j,\mathbf{k}} = E^\dagger_{j,\mathbf{k}} E_{j,\mathbf{k}} = \omega_{j,\mathbf{k}} N_{j,\mathbf{k}}$, so that $\langle H_j\rangle = \mathrm{Tr}[\sum_{\mathbf{k}} E^\dagger_{j,\mathbf{k}} E_{j,\mathbf{k}}\hat\rho]/Z$. Introducing $\omega = k$ as integration variable and writing $\hat T_{j,\mathbf{k}} = \hat T_j(\omega, \mathbf{k}_0)$, we find the spectral representation of the internal energy $\langle H\rangle = \langle H_1\rangle + \langle H_2\rangle$ in the thermodynamic limit,

$$\frac{\langle H_j\rangle}{L^3} = \int \mathrm{d}\rho_j(\omega,\mathbf{k}_0), \quad \mathrm{d}\rho_j(\omega,\mathbf{k}_0) = \rho_j(\omega,\mathbf{k}_0)\mathrm{d}\omega\mathrm{d}\Omega_{\mathbf{k}_0},$$
$$\rho_j(\omega,\mathbf{k}_0) = \langle E^\dagger_{j,\mathbf{k}} E_{j,\mathbf{k}}\rangle = \frac{1}{(2\pi)^3}\frac{\omega^3}{\mathrm{e}^{\omega/\hat T_j(\omega,\mathbf{k}_0)}-1}, \tag{2.11}$$

where $\mathrm{d}\Omega_{\mathbf{k}_0}$ is the surface element of the unit sphere, $\mathrm{d}\Omega_{\mathbf{k}_0} = \sin\theta\mathrm{d}\theta\mathrm{d}\phi$; the $\rho_j(\omega,\mathbf{k}_0)$ are spectral intensities per steradian ($\hbar = c = k_\mathrm{B} = 1$), and we will occasionally use the shortcut $\rho_{j,\mathbf{k}}$ for $\rho_j(\omega,\mathbf{k}_0)$, with $\omega = k$.

The entropy $\langle S\rangle = -\mathrm{Tr}[\hat\rho_S \log\hat\rho_S]$ is defined by the normalized density operator $\hat\rho_S = \hat\rho/Z$, $\hat\rho = \exp(-H_{\hat T})$, see after (2.4), so that $\mathrm{Tr}[\hat\rho_S] = 1$ and $\langle S\rangle = \log Z + \langle H_{\hat T}\rangle$. The thermodynamic limit of $\log Z$ is stated in (2.9), with $\varepsilon = 0$ and $f_{j,\mathbf{k}} = \omega_{j,\mathbf{k}}/\hat T_{j,\mathbf{k}}$, cf. (2.5). The expectation value $\langle H_{\hat T}\rangle$ is given by $\langle G\rangle$ in (2.10) with $g_{j,\mathbf{k}} = \omega_{j,\mathbf{k}}/\hat T_{j,\mathbf{k}}$, cf. (2.5), and is not to be confused with the internal energy $\langle H\rangle$, see after (2.10).

2.2. Variances and higher-order correlations

We consider random variables $G^{(n)}$, $n = 1,\ldots,\widetilde N$, defined by operators

$$G^{(n)} = \sum_{j,\mathbf{k}}\Big(g^{(n)}_{j,\mathbf{k}} N_{j,\mathbf{k}} + \frac{c^{(n)}_{j,\mathbf{k}}}{2}\Big), \tag{2.12}$$

where the $g^{(n)}_{j,\mathbf{k}}$ and $c^{(n)}_{j,\mathbf{k}}$ are arbitrary functions and the $N_{j,\mathbf{k}}$ particle number operators as in (2.3). The partition function reads

$$Z = \mathrm{Tr}[\hat\rho(\varepsilon_1,\ldots,\varepsilon_{\widetilde N})], \quad \hat\rho(\varepsilon_1,\ldots,\varepsilon_{\widetilde N}) = \exp\Big(-H_{\hat T} - \sum_{n=1}^{\widetilde N}\varepsilon_n G^{(n)}\Big), \tag{2.13}$$

with $H_{\hat T}$ defined after (2.4). The ε_n, $n = 1,\ldots,\widetilde N$, are dimensionless and put to zero after differentiation. The expectation values are thus $\langle G^{(n)}\rangle = -(\log Z)_{,\varepsilon_n} = \mathrm{Tr}[G^{(n)}\hat\rho]/Z$.

We write the exponent of the density operator in (2.13) as

$$H_{\hat T} + \sum_{n=1}^{\widetilde N}\varepsilon_n G^{(n)} = \sum_{j,\mathbf{k}}(\alpha_{j,\mathbf{k}} N_{j,\mathbf{k}} + \beta_{j,\mathbf{k}}/2),$$
$$\alpha_{j,\mathbf{k}} = \frac{\omega_{j,\mathbf{k}}}{\hat T_{j,\mathbf{k}}} + \sum_{n=1}^{\widetilde N}\varepsilon_n g^{(n)}_{j,\mathbf{k}}, \quad \beta_{j,\mathbf{k}} = \frac{\omega_{j,\mathbf{k}}}{\hat T_{j,\mathbf{k}}} + \sum_{n=1}^{\widetilde N}\varepsilon_n c^{(n)}_{j,\mathbf{k}}. \tag{2.14}$$

The partition function can be evaluated as in (2.6) and (2.7). Performing the continuum limit, we obtain, cf. (2.9) and (2.10),

$$\log Z = -\frac{L^3}{(2\pi)^3}\sum_{j=1}^{2}\int\Big(\frac{\beta_{j,\mathbf{k}}}{2} + \log(1-\mathrm{e}^{-\alpha_{j,\mathbf{k}}})\Big)\mathrm{d}\mathbf{k}, \tag{2.15}$$

and the expectation values are

$$\langle G^{(n)}\rangle = -(\log Z)_{,\varepsilon_n} = \frac{L^3}{(2\pi)^3}\sum_{j=1}^{2}\int\Big(\frac{g^{(n)}_{j,\mathbf{k}}}{\mathrm{e}^{\omega_{j,\mathbf{k}}/\hat T_{j,\mathbf{k}}}-1} + \frac{c^{(n)}_{j,\mathbf{k}}}{2}\Big)\mathrm{d}\mathbf{k}. \tag{2.16}$$

For instance, if we choose $G^{(1)} = H$, we can identify $g^{(1)}_{j,\mathbf{k}} = c^{(1)}_{j,\mathbf{k}} = \omega_{j,\mathbf{k}}$. If we put $G^{(2)} = \log Z_{\varepsilon=0} + H_{\hat T}$, with $\log Z_{\varepsilon=0}$ in (2.9), we can identify $g^{(2)}_{j,\mathbf{k}} = \omega_{j,\mathbf{k}}/\hat T_{j,\mathbf{k}}$ and $c^{(2)}_{j,\mathbf{k}} = -2\log(1-\mathrm{e}^{-\omega_{j,\mathbf{k}}/\hat T_{j,\mathbf{k}}})$ to recover the entropy $\langle S\rangle = \langle G^{(2)}\rangle = \mathrm{Tr}[G^{(2)}\hat\rho]/Z$, see after (2.11). In the following, we will mostly put $c^{(n)}_{j,\mathbf{k}} = 0$ in (2.12) and (2.16), since these coefficients usually lead to zero-point singularities when integrated.

Regarding fluctuations of the random variables (2.12), we use the shortcut $\Delta G^{(n)} = G^{(n)} - \langle G^{(n)}\rangle$. Variances and covariances are calculated via $\langle\Delta G^{(n)}\Delta G^{(m)}\rangle = \langle G^{(n)}G^{(m)}\rangle - \langle G^{(n)}\rangle\langle G^{(m)}\rangle = (\log Z)_{,\varepsilon_n,\varepsilon_m}$, and higher-order correlations are assembled analogously, $\langle\Delta G^{(n)}\Delta G^{(m)}\Delta G^{(l)}\rangle = -(\log Z)_{,\varepsilon_n,\varepsilon_m,\varepsilon_l}$; the minus sign arises in the case of an odd number of factors [23,24]. We note the ratio

$$\frac{\langle\Delta G^{(n)}\Delta G^{(m)}\rangle}{\langle G^{(n)}\rangle\langle G^{(m)}\rangle} = \frac{\langle G^{(n)}G^{(m)}\rangle}{\langle G^{(n)}\rangle\langle G^{(m)}\rangle} - 1 = \frac{(\log Z)_{,\varepsilon_n,\varepsilon_m}}{(\log Z)_{,\varepsilon_m}(\log Z)_{,\varepsilon_n}} \propto \frac{1}{L^3}. \tag{2.17}$$

Thus $\langle G^{(n)}G^{(m)}\rangle$ factorizes as $\langle G^{(n)}\rangle\langle G^{(m)}\rangle$ in the thermodynamic limit $V\to\infty$. This applies to variables structured as in (2.12). Moreover, their relative fluctuations vanish, since $\sqrt{\langle(\Delta G^{(n)})^2\rangle}/\langle G^{(n)}\rangle\propto 1/\sqrt{L^3}$.

3. Polarized electric field strengths in second quantization

3.1. Expectation values defining the Stokes parameters

To describe polarization, we introduce a new set of annihilation and creation operators $b_{j,\mathbf{k}}$ and $b^\dagger_{j,\mathbf{k}}$, by applying a unitary rotation to the $a_{j,\mathbf{k}}$ defined in Section 2.1,

$$\begin{pmatrix}b_{1,\mathbf{k}}\\ b_{2,\mathbf{k}}\end{pmatrix}=\mathrm{e}^{\mathrm{i}\delta_{\mathbf{k}}}\begin{pmatrix}\mathrm{e}^{\mathrm{i}\eta_{\mathbf{k}}}\cos\psi_{\mathbf{k}} & -\mathrm{e}^{-\mathrm{i}(\chi_{\mathbf{k}}+\eta_{\mathbf{k}})}\sin\psi_{\mathbf{k}}\\ \mathrm{e}^{\mathrm{i}(\chi_{\mathbf{k}}+\eta_{\mathbf{k}})}\sin\psi_{\mathbf{k}} & \mathrm{e}^{-\mathrm{i}\eta_{\mathbf{k}}}\cos\psi_{\mathbf{k}}\end{pmatrix}\begin{pmatrix}a_{1,\mathbf{k}}\\ a_{2,\mathbf{k}}\end{pmatrix}. \tag{3.1}$$

The indicated matrix is the most general two-by-two unitary matrix, with determinant $\mathrm{e}^{2\mathrm{i}\delta_{\mathbf{k}}}$. (The phase factor $\mathrm{e}^{\mathrm{i}\delta_{\mathbf{k}}}$ can be put to one from the outset, unless we consider space reflections changing the orientation of the polarization triad $\boldsymbol{\varepsilon}_{j=1,2}$, $\mathbf{k}_0$, cf. after (2.1).) The $b_{j,\mathbf{k}}$ and their adjoints satisfy the same commutation relations as the $a_{j,\mathbf{k}}$, cf. after (2.2), and we note the expectation values

$$\begin{aligned}\langle b_1^\dagger b_1\rangle &= \langle a_1^\dagger a_1\rangle\cos^2\psi+\langle a_2^\dagger a_2\rangle\sin^2\psi,\quad \langle b_1^\dagger b_2\rangle=(\langle a_1^\dagger a_1\rangle-\langle a_2^\dagger a_2\rangle)\mathrm{e}^{\mathrm{i}\chi}\sin\psi\cos\psi\\ \langle b_2^\dagger b_1\rangle &= (\langle a_1^\dagger a_1\rangle-\langle a_2^\dagger a_2\rangle)\mathrm{e}^{-\mathrm{i}\chi}\sin\psi\cos\psi,\quad \langle b_2^\dagger b_2\rangle=\langle a_1^\dagger a_1\rangle\sin^2\psi+\langle a_2^\dagger a_2\rangle\cos^2\psi,\end{aligned} \tag{3.2}$$

where we have suppressed the $\mathbf{k}$ subscript on the operators and angles. The phases $\mathrm{e}^{\mathrm{i}\delta}$ and $\mathrm{e}^{\mathrm{i}\eta}$ of transformation (3.1) drop out in (3.2), and the angle ψ and phase $\mathrm{e}^{\mathrm{i}\chi}$ can be determined by measuring the Stokes parameters, see (3.10). The polarized field strength $\hat{\mathbf{E}}(\mathbf{x},t)$ is defined like $\mathbf{E}(\mathbf{x},t)$ in (2.1), with the operators $a_{j,\mathbf{k}}$ replaced by the $b_{j,\mathbf{k}}$ in (3.1),

$$\begin{aligned}\hat{\mathbf{E}}(\mathbf{x},t)&=\frac{1}{\sqrt{2L^3}}\sum_{\mathbf{k}}(\hat{\mathbf{E}}_{\mathbf{k}}\mathrm{e}^{\mathrm{i}(\mathbf{k}\mathbf{x}-\omega t)}+\hat{\mathbf{E}}^\dagger_{\mathbf{k}}\mathrm{e}^{-\mathrm{i}(\mathbf{k}\mathbf{x}-\omega t)}),\\ \hat{\mathbf{E}}_{\mathbf{k}}&=\boldsymbol{\varepsilon}_1\hat{E}_{1,\mathbf{k}}+\boldsymbol{\varepsilon}_2\hat{E}_{2,\mathbf{k}},\quad \hat{E}_{j,\mathbf{k}}=\sqrt{\omega_{j,\mathbf{k}}}b_{j,\mathbf{k}},\end{aligned} \tag{3.3}$$

where $\boldsymbol{\varepsilon}_{j=1,2}$ and $\mathbf{k}_0$ define the polarization triad. The polarized field amplitudes $\hat{E}_{j,\mathbf{k}}$ are thus related to the normalized annihilation operators $E_{j,\mathbf{k}}=\sqrt{\omega_{j,\mathbf{k}}}a_{j,\mathbf{k}}$ in (2.1) by the unitary transform

$$\begin{aligned}\hat{E}_1&=\mathrm{e}^{\mathrm{i}\delta}(E_1\mathrm{e}^{\mathrm{i}\eta}\cos\psi-E_2\mathrm{e}^{-\mathrm{i}\eta}\mathrm{e}^{-\mathrm{i}\chi}\sin\psi),\\ \hat{E}_2&=\mathrm{e}^{\mathrm{i}\delta}(E_1\mathrm{e}^{\mathrm{i}\eta}\mathrm{e}^{\mathrm{i}\chi}\sin\psi+E_2\mathrm{e}^{-\mathrm{i}\eta}\cos\psi),\end{aligned} \tag{3.4}$$

where we again suppressed the $\mathbf{k}$ subscript. The expectation values of the products $\hat{E}^\dagger_{i,\mathbf{k}}\hat{E}_{j,\mathbf{k}}$ of the field amplitudes $\hat{E}_{j,\mathbf{k}}$ (defining the field strength in the $\boldsymbol{\varepsilon}_{j=1,2}$ directions) read, cf. (2.11) and (3.2),

$$\begin{aligned}\langle\hat{E}^\dagger_{1,\mathbf{k}}\hat{E}_{1,\mathbf{k}}\rangle&=\rho_1\cos^2\psi+\rho_2\sin^2\psi,\quad \langle\hat{E}^\dagger_{2,\mathbf{k}}\hat{E}_{1,\mathbf{k}}\rangle=(\rho_1-\rho_2)\mathrm{e}^{-\mathrm{i}\chi}\sin\psi\cos\psi,\\ \langle\hat{E}^\dagger_{1,\mathbf{k}}\hat{E}_{2,\mathbf{k}}\rangle&=(\rho_1-\rho_2)\mathrm{e}^{\mathrm{i}\chi}\sin\psi\cos\psi,\quad \langle\hat{E}^\dagger_{2,\mathbf{k}}\hat{E}_{2,\mathbf{k}}\rangle=\rho_1\sin^2\psi+\rho_2\cos^2\psi,\end{aligned} \tag{3.5}$$

where $\rho_j(\omega,\mathbf{k}_0)$ denotes the spectral density (2.11). Using the double-angle formulas $\sin\psi\cos\psi=\sin 2\psi/2$, $\sin^2\psi=(1-\cos 2\psi)/2$ and $\cos^2\psi=(1+\cos 2\psi)/2$, we can write this as

$$\begin{aligned}\langle\hat{E}^\dagger_{1,\mathbf{k}}\hat{E}_{1,\mathbf{k}}\rangle&=(\rho_1+\rho_2)/2+(\rho_1-\rho_2)\cos 2\psi/2,\\ \langle\hat{E}^\dagger_{2,\mathbf{k}}\hat{E}_{2,\mathbf{k}}\rangle&=(\rho_1+\rho_2)/2-(\rho_1-\rho_2)\cos 2\psi/2,\\ \langle\hat{E}^\dagger_{2,\mathbf{k}}\hat{E}_{1,\mathbf{k}}\rangle&=(\rho_1-\rho_2)\mathrm{e}^{-\mathrm{i}\chi}\sin 2\psi/2,\quad \langle\hat{E}^\dagger_{1,\mathbf{k}}\hat{E}_{2,\mathbf{k}}\rangle=(\rho_1-\rho_2)\mathrm{e}^{\mathrm{i}\chi}\sin 2\psi/2.\end{aligned} \tag{3.6}$$

These expectation values define the polarization matrix [25]

$$p_{ij}=\begin{pmatrix}\langle\hat{E}^\dagger_{1,\mathbf{k}}\hat{E}_{1,\mathbf{k}}\rangle & \langle\hat{E}^\dagger_{2,\mathbf{k}}\hat{E}_{1,\mathbf{k}}\rangle\\ \langle\hat{E}^\dagger_{1,\mathbf{k}}\hat{E}_{2,\mathbf{k}}\rangle & \langle\hat{E}^\dagger_{2,\mathbf{k}}\hat{E}_{2,\mathbf{k}}\rangle\end{pmatrix}=\frac{1}{2}\begin{pmatrix}I_{\mathbf{k}}+Q_{\mathbf{k}} & U_{\mathbf{k}}+\mathrm{i}V_{\mathbf{k}}\\ U_{\mathbf{k}}-\mathrm{i}V_{\mathbf{k}} & I_{\mathbf{k}}-Q_{\mathbf{k}}\end{pmatrix}, \tag{3.7}$$

which is hermitian with trace $\rho_1+\rho_2$ (total intensity I) and determinant $\rho_1\rho_2$. Also indicated in (3.7) are the Stokes parameters I, Q, U and V, and we note $Q^2+U^2+V^2=\mathrm{tr}^2(p_{ij})-4\det p_{ij}$. Inversely,

$$\begin{aligned}I&=\langle\hat{E}_1^\dagger\hat{E}_1\rangle+\langle\hat{E}_2^\dagger\hat{E}_2\rangle,\quad Q=\langle\hat{E}_1^\dagger\hat{E}_1\rangle-\langle\hat{E}_2^\dagger\hat{E}_2\rangle,\\ U&=\langle\hat{E}_2^\dagger\hat{E}_1\rangle+\langle\hat{E}_1^\dagger\hat{E}_2\rangle,\quad V=-\mathrm{i}(\langle\hat{E}_2^\dagger\hat{E}_1\rangle-\langle\hat{E}_1^\dagger\hat{E}_2\rangle),\end{aligned} \tag{3.8}$$

where we have dropped the $\mathbf{k}$ subscript. We thus find, by way of (3.6), $I=\rho_1+\rho_2$ and

$$Q=\delta\rho\cos 2\psi,\quad U=2\delta\rho\cos\chi\sin 2\psi,\quad V=-2\delta\rho\sin\chi\sin 2\psi, \tag{3.9}$$

with the shortcut $\delta\rho = \rho_1 - \rho_2$. We also note the consistency condition $\mathrm{sign}(U\cos\chi) = -\mathrm{sign}(V\sin\chi)$. A solution of Eqs. (3.9) is

$$\delta\rho = \rho_1 - \rho_2 = \sqrt{Q^2+U^2+V^2}, \quad \mathrm{e}^{\mathrm{i}\chi} = \frac{U-\mathrm{i}V}{\sqrt{U^2+V^2}},$$
$$\sin 2\psi = \frac{\sqrt{U^2+V^2}}{\sqrt{Q^2+U^2+V^2}}, \quad \cos 2\psi = \frac{Q}{\sqrt{Q^2+U^2+V^2}}. \tag{3.10}$$

There are three other solutions of (3.9); the second is obtained by changing the sign of $\delta\rho$, $\sin 2\psi$ and $\cos 2\psi$, the third by changing the sign of $\mathrm{e}^{\mathrm{i}\chi}$ and $\sin 2\psi$, and the fourth by changing the sign of $\mathrm{e}^{\mathrm{i}\chi}$, $\delta\rho$ and $\cos 2\psi$. We will use solution (3.10), which implies $\rho_1 \geq \rho_2$ and determines the angles unambiguously in the range $0 \leq \psi \leq \pi/2$ and $-\pi < \chi \leq \pi$, so that $\sin\psi = \sqrt{(1-\cos 2\psi)/2}$ and $\cos\psi = \sqrt{(1+\cos 2\psi)/2}$. In this way, we can express ψ and the phase factor $\mathrm{e}^{\mathrm{i}\chi}$ in (3.4) in terms of Stokes parameters. The factors $\mathrm{e}^{\mathrm{i}\delta}$ and $\mathrm{e}^{\mathrm{i}\eta}$ of the unitary transform (3.4) do not enter in the expectation values defining the polarization matrix (3.7). Totally unpolarized radiation $Q = U = V = 0$ corresponds to $\psi = \chi = 0$, so that $\hat{E}_{1,\mathbf{k}} = E_{1,\mathbf{k}}\mathrm{e}^{\mathrm{i}(\delta+\eta)}$, $\hat{E}_{2,\mathbf{k}} = E_{2,\mathbf{k}}\mathrm{e}^{\mathrm{i}(\delta-\eta)}$, cf. (3.4); also see Section 3.4.

3.2. Angular temperature and polarization fluctuations extracted from the Stokes parameters

To relate the temperature variables $\hat{T}_{j,\mathbf{k}} = \hat{T}_j(\omega,\mathbf{k}_0)$ of the spectral densities $\rho_{j,\mathbf{k}} = \rho_j(\omega,\mathbf{k}_0)$ in (2.11) to the Stokes parameters, we use $\rho_1+\rho_2 = I$ and $\rho_1-\rho_2 = \sqrt{Q^2+U^2+V^2}$, cf. after (3.8) and (3.10),

$$\rho_{1,\mathbf{k}} = \frac{1}{2}(I_{\mathbf{k}} + \sqrt{Q_{\mathbf{k}}^2+U_{\mathbf{k}}^2+V_{\mathbf{k}}^2}), \quad \rho_{2,\mathbf{k}} = \frac{1}{2}(I_{\mathbf{k}} - \sqrt{Q_{\mathbf{k}}^2+U_{\mathbf{k}}^2+V_{\mathbf{k}}^2}). \tag{3.11}$$

The $\rho_{j,\mathbf{k}}$ are the eigenvalues of the polarization matrix p_{ij} in (3.7). By inverting the spectral density $\rho_{j,\mathbf{k}} = \rho_j(\omega,\mathbf{k}_0)$ in (2.11), we find

$$\hat{T}_j(\omega,\mathbf{k}_0) = \frac{\omega}{\log(1+\omega^3/((2\pi)^3\rho_{j,\mathbf{k}}))}, \tag{3.12}$$

with $\rho_{j,\mathbf{k}}$ parametrized as in (3.11). $\hat{T}_j(\omega,\mathbf{k}_0)$ can thus be extracted from the measured Stokes parameters. We also note $\hat{T}_1 \geq \hat{T}_2$, since $\rho_1-\rho_2 \geq 0$ by definition. In the case of the CMB radiation, $\hat{T}_j(\omega,\mathbf{k}_0)$ is frequency independent.

We split off the angular-dependent fluctuating part of the temperature, $\hat{T}_j(\omega,\mathbf{k}_0) = \hat{T}_{0,j} + \delta\hat{T}_j(\omega,\mathbf{k}_0)$, where $\hat{T}_{0,j}$ is the angular-averaged temperature $\hat{T}_{0,j} = \int \hat{T}_j(\omega,\mathbf{k}_0)\mathrm{d}\Omega_{\mathbf{k}_0}/(4\pi)$ of the respective polarization component labeled $j = 1, 2$, and write

$$\hat{T}_1(\omega,\mathbf{k}_0) = T_0 + P_0 + T_{\mathbf{k}} + P_{\mathbf{k}}, \quad \hat{T}_2(\omega,\mathbf{k}_0) = T_0 - P_0 + T_{\mathbf{k}} - P_{\mathbf{k}}, \tag{3.13}$$

where

$$T_0 = (\hat{T}_{0,1}+\hat{T}_{0,2})/2, \quad P_0 = (\hat{T}_{0,1}-\hat{T}_{0,2})/2,$$
$$T_{\mathbf{k}} = (\delta\hat{T}_1+\delta\hat{T}_2)/2, \quad P_{\mathbf{k}} = (\delta\hat{T}_1-\delta\hat{T}_2)/2. \tag{3.14}$$

We also note $P_0 \geq 0$ and $P_0+P_{\mathbf{k}} \geq 0$ since $\hat{T}_1 \geq \hat{T}_2$, and $\int T_{\mathbf{k}}\mathrm{d}\Omega_{\mathbf{k}_0} = \int P_{\mathbf{k}}\mathrm{d}\Omega_{\mathbf{k}_0} = 0$. If the temperatures $\hat{T}_j(\omega,\mathbf{k}_0)$ are frequency and angular independent, so that $\hat{T}_{1,2} = T_0 \pm P_0$, they define two Planckians (2.11) whose superposition $\rho_1+\rho_2$ gives an isotropic polarized spectral density. If the mean polarization P_0 is negligible compared with the mean temperature T_0, the densities ρ_1 and ρ_2 become identical, resulting in unpolarized isotropic black-body radiation.

3.3. Expansion of the spectral density in angular fluctuations

We write the spectral intensities (2.11) as, cf. (3.13),

$$\rho_{j,\mathbf{k}} = \frac{1}{(2\pi)^3}\frac{\omega^3}{\mathrm{e}^{\omega/(T_0\pm P_0+T_{\mathbf{k}}\pm P_{\mathbf{k}})}-1}, \tag{3.15}$$

and assume the temperature fluctuations $T_{\mathbf{k}}$ and polarization $P_0+P_{\mathbf{k}}$ to be much smaller than the mean temperature T_0, cf. (3.14). We denote the isotropic unpolarized Planckian by

$$\rho^{\mathrm{iso}} = \frac{1}{(2\pi)^3}\frac{\omega^3}{\mathrm{e}^{\omega/T_0}-1}, \tag{3.16}$$

and expand density $\rho_{j,\mathbf{k}}$ in (3.15) to second order in the fluctuations,

$$\rho_{j,\mathbf{k}} = \rho^{\mathrm{iso}} + \rho^{\mathrm{iso}}_{,T_0}(T_{\mathbf{k}} \pm (P_0+P_{\mathbf{k}})) + \frac{1}{2}\rho^{\mathrm{iso}}_{,T_0,T_0}(T_{\mathbf{k}} \pm (P_0+P_{\mathbf{k}}))^2, \tag{3.17}$$

to find

$$\rho_{1,\mathbf{k}}+\rho_{2,\mathbf{k}}=2\rho^{\rm iso}+2\rho^{\rm iso}_{,T_0}T_{\mathbf{k}}+\rho^{\rm iso}_{,T_0,T_0}(T^2_{\mathbf{k}}+(P_0+P_{\mathbf{k}})^2),$$
$$\delta\rho_{\mathbf{k}}=\rho_{1,\mathbf{k}}-\rho_{2,\mathbf{k}}=2\rho^{\rm iso}_{,T_0}(P_0+P_{\mathbf{k}})+2\rho^{\rm iso}_{,T_0,T_0}T_{\mathbf{k}}(P_0+P_{\mathbf{k}}). \tag{3.18}$$

Thus, in linear order, the polarization is related to the Stokes parameters by $P_0+P_{\mathbf{k}}\sim\sqrt{Q^2_{\mathbf{k}}+U^2_{\mathbf{k}}+V^2_{\mathbf{k}}}/(2\rho^{\rm iso}_{,T_0})$, cf. (3.10). Since the temperature and polarization fluctuations $T_{\mathbf{k}}$ and $P_0+P_{\mathbf{k}}$ are invariant under rotations of the polarization vectors, they can be expanded in scalar spherical harmonics. In the case of the CMB radiation, the V parameter generating elliptical/circular polarization has not been measured and is assumed to be negligible.

3.4. Decomposition of the spectral density into totally polarized and unpolarized components

The polarization matrix (3.7) can be decomposed into an unpolarized and a totally polarized component [25],

$$p_{ij}=\frac{1}{2}\begin{pmatrix} I_{\rm unpol} & 0\\ 0 & I_{\rm unpol}\end{pmatrix}+\frac{1}{2}\begin{pmatrix} I_{\rm totpol}+Q & U+{\rm i}V\\ U-{\rm i}V & I_{\rm totpol}-Q\end{pmatrix}, \tag{3.19}$$

with intensities

$$I_{\rm unpol}=2\rho_2=I-\sqrt{Q^2+U^2+V^2},\quad I_{\rm totpol}=\rho_1-\rho_2=\sqrt{Q^2+U^2+V^2}. \tag{3.20}$$

The determinant of the second matrix in (3.19) vanishes, which is the condition defining the totally polarized intensity $I_{\rm totpol}$. Linear polarization implies $V=0$, and circular polarization $Q=U=0$. The second-order fluctuation expansions of the intensities $I_{\rm unpol}=2\rho_2$ and $I_{\rm totpol}=\rho_1-\rho_2$ are stated in (3.17) and (3.18). In Section 5.3, we will perform the angular fluctuation average of $I_{\rm unpol}$ and $I_{\rm totpol}$ to estimate the polarization degree.

4. Spatial correlation functions

4.1. Two-point correlations of the electric field strength

We start with the Fourier series of the electric field in (2.1), and consider the product

$$\mathbf{E}(\mathbf{x},t)\mathbf{E}(\mathbf{y},t)=\frac{1}{2L^3}\sum_{i,\mathbf{k},\mathbf{k}'}(E^\dagger_{i,\mathbf{k}}E_{i,\mathbf{k}'}{\rm e}^{-{\rm i}(\mathbf{k}\mathbf{x}-\omega_{\mathbf{k}}t)}{\rm e}^{{\rm i}(\mathbf{k}'\mathbf{y}-\omega_{\mathbf{k}'}t)}+E_{i,\mathbf{k}}E^\dagger_{i,\mathbf{k}'}{\rm e}^{{\rm i}(\mathbf{k}\mathbf{x}-\omega_{\mathbf{k}}t)}{\rm e}^{-{\rm i}(\mathbf{k}'\mathbf{y}-\omega_{\mathbf{k}'}t)}), \tag{4.1}$$

with the quantized amplitudes $E_{j,\mathbf{k}}=\sqrt{\omega_{j,\mathbf{k}}}a_{j,\mathbf{k}}$, $E^\dagger_{j,\mathbf{k}}=\sqrt{\omega_{j,\mathbf{k}}}a^\dagger_{j,\mathbf{k}}$, cf. after (2.2). Using the commutation relation $[a_i,a^\dagger_n]=\delta_{in}$, we can write this as

$$\begin{aligned}\mathbf{E}(\mathbf{x},t)\mathbf{E}(\mathbf{y},t)=&\frac{1}{2L^3}\sum_{i,\mathbf{k},\mathbf{k}'}\sqrt{\omega_{i,\mathbf{k}}\omega_{i,\mathbf{k}'}}a^\dagger_{i,\mathbf{k}}a_{i,\mathbf{k}'}({\rm e}^{-{\rm i}\mathbf{k}\mathbf{x}}{\rm e}^{{\rm i}\mathbf{k}'\mathbf{y}}+{\rm e}^{{\rm i}\mathbf{k}'\mathbf{x}}{\rm e}^{-{\rm i}\mathbf{k}\mathbf{y}}){\rm e}^{{\rm i}(\omega_{\mathbf{k}}-\omega_{\mathbf{k}'})t}\\&+\frac{1}{2L^3}\sum_{i,\mathbf{k}}\omega_{i,\mathbf{k}}{\rm e}^{{\rm i}\mathbf{k}(\mathbf{x}-\mathbf{y})}.\end{aligned} \tag{4.2}$$

The off-diagonal terms in (4.2) drop out when taking the expectation value, cf. (2.4),

$$\langle\mathbf{E}(\mathbf{x},t)\mathbf{E}(\mathbf{y},t)\rangle=\frac{1}{2L^3}\langle\sum_{i,\mathbf{k}}\omega_{i,\mathbf{k}}N_{i,\mathbf{k}}({\rm e}^{{\rm i}\mathbf{k}(\mathbf{x}-\mathbf{y})}+{\rm c.c})\rangle+\frac{1}{2L^3}\sum_{i,\mathbf{k}}\omega_{i,\mathbf{k}}{\rm e}^{{\rm i}\mathbf{k}(\mathbf{x}-\mathbf{y})}. \tag{4.3}$$

Performing the continuum limit, cf. (2.10) and (2.11), we find

$$\langle\mathbf{E}(\mathbf{x},t)\mathbf{E}(\mathbf{y},t)\rangle=\int\langle\mathbf{E}(\mathbf{x},t)\mathbf{E}(\mathbf{y},t)\rangle_{\mathbf{k}}{\rm d}\omega{\rm d}\Omega_{\mathbf{k}_0}, \tag{4.4}$$

where ${\rm d}\Omega_{\mathbf{k}_0}$ is the solid angle element, and the spectral kernel reads

$$\langle\mathbf{E}(\mathbf{x},t)\mathbf{E}(\mathbf{y},t)\rangle_{\mathbf{k}}=\frac{1}{2}({\rm e}^{-{\rm i}\mathbf{k}(\mathbf{x}-\mathbf{y})}+{\rm e}^{{\rm i}\mathbf{k}(\mathbf{x}-\mathbf{y})})\sum_j\rho_{j,\mathbf{k}}+\frac{1}{(2\pi)^3}\omega^3{\rm e}^{{\rm i}\mathbf{k}(\mathbf{x}-\mathbf{y})}, \tag{4.5}$$

with $\rho_{j,\mathbf{k}}=\rho_j(\omega,\mathbf{k}_0)$ as in (2.11) and $\omega=k$. Evidently, $\langle\mathbf{E}^2(\mathbf{x},t)\rangle=(\langle H_1\rangle+\langle H_2\rangle)/L^3$, cf. (2.11).

If the temperature $\hat{T}_{j,\mathbf{k}}$ defining density $\rho_{j,\mathbf{k}}$ in (2.11) is independent of $\mathbf{k}_0$, see after (3.14), we can perform the angular integration in (4.4) using $\int{\rm e}^{\pm{\rm i}\mathbf{k}\mathbf{x}}{\rm d}\Omega_{\mathbf{k}_0}=4\pi\sin(kr)/(kr)$, to find [26]

$$\langle\mathbf{E}(\mathbf{x},t)\mathbf{E}(\mathbf{y},t)\rangle=\frac{4\pi}{(2\pi)^3}\sum_j\int_0^\infty\frac{\sin(\omega r)}{\omega r}(\frac{1}{{\rm e}^{\omega/\hat{T}_j}-1}+\frac{1}{2})\omega^3{\rm d}\omega, \tag{4.6}$$

with $r=|\mathbf{x}-\mathbf{y}|$. The second term in the parentheses results in a zero-point divergence, cf. (2.10), and can be dropped.

4.2. Energy density correlations of an anisotropic and partially polarized photon gas

We specialize the Fourier series of the product $\mathbf{E}(\mathbf{x},t)\mathbf{E}(\mathbf{y},t)$ in (4.2) to $\mathbf{y}=\mathbf{x}$ and consider the fluctuation variable $\Delta\mathbf{E}^2(\mathbf{x},t)=\mathbf{E}^2(\mathbf{x},t)-\langle\mathbf{E}^2(\mathbf{x},t)\rangle$, cf. (4.4) and (4.5),

$$\Delta\mathbf{E}^2(\mathbf{x},t)=\frac{1}{L^3}\sum_{i,\mathbf{k}\neq\mathbf{k}'}\sqrt{\omega_{i,\mathbf{k}}\omega_{i,\mathbf{k}'}}a^\dagger_{i,\mathbf{k}}a_{i,\mathbf{k}'}\mathrm{e}^{-\mathrm{i}(\mathbf{k}\mathbf{x}-\omega_{\mathbf{k}}t)}\mathrm{e}^{\mathrm{i}(\mathbf{k}'\mathbf{x}-\omega_{\mathbf{k}'}t)}. \tag{4.7}$$

The expectation value of the product $\Delta\mathbf{E}^2(\mathbf{x},t)\Delta\mathbf{E}^2(\mathbf{y},t)$ reads [27]

$$\begin{aligned}\langle\Delta\mathbf{E}^2(\mathbf{x},t)\Delta\mathbf{E}^2(\mathbf{y},t)\rangle &= \sum_j\langle\frac{1}{L^3}\sum_{\mathbf{k}}\omega_{\mathbf{k}}N_{j,\mathbf{k}}\mathrm{e}^{-\mathrm{i}\mathbf{k}(\mathbf{x}-\mathbf{y})}\rangle\langle\frac{1}{L^3}\sum_{\mathbf{p}}\omega_{\mathbf{p}}N_{j,\mathbf{p}}\mathrm{e}^{\mathrm{i}\mathbf{p}(\mathbf{x}-\mathbf{y})}\rangle\\ &+\frac{1}{L^3}\sum_{\mathbf{p}}\omega_{\mathbf{p}}\mathrm{e}^{\mathrm{i}\mathbf{p}(\mathbf{x}-\mathbf{y})}\sum_j\langle\frac{1}{L^3}\sum_{\mathbf{k}}\omega_{\mathbf{k}}N_{j,\mathbf{k}}\mathrm{e}^{-\mathrm{i}\mathbf{k}(\mathbf{x}-\mathbf{y})}\rangle,\end{aligned} \tag{4.8}$$

where we applied the commutation relation $[a_{i,\mathbf{k}},a^\dagger_{j,\mathbf{p}}]=\delta_{ij}\delta_{\mathbf{kp}}$, cf. after (2.2), and factorized according to (2.17). In the continuum limit, this reads

$$\begin{aligned}\langle\Delta\mathbf{E}^2(\mathbf{x},t)\Delta\mathbf{E}^2(\mathbf{y},t)\rangle &= \sum_j\int\mathrm{e}^{-\mathrm{i}\mathbf{k}(\mathbf{x}-\mathbf{y})}\mathrm{d}\rho_j(\omega,\mathbf{k}_0)\int\mathrm{e}^{\mathrm{i}\mathbf{p}(\mathbf{x}-\mathbf{y})}\mathrm{d}\rho_j(\omega,\mathbf{p}_0)\\ &+\frac{1}{(2\pi)^3}\int\omega_{\mathbf{p}}\mathrm{e}^{\mathrm{i}\mathbf{p}(\mathbf{x}-\mathbf{y})}\mathrm{d}\mathbf{p}\sum_j\int\mathrm{e}^{-\mathrm{i}\mathbf{k}(\mathbf{x}-\mathbf{y})}\mathrm{d}\rho_j(\omega,\mathbf{k}_0),\end{aligned} \tag{4.9}$$

with spectral density $\mathrm{d}\rho_j(\omega,\mathbf{k}_0)=\rho_j(\omega,\mathbf{k}_0)\mathrm{d}\omega\mathrm{d}\Omega_{\mathbf{k}_0}$ in (2.11) and $\omega_{\mathbf{p}}=p$. The first series in (4.9) is the actual correlation function; the second term in (4.9) has a zero-point divergence due to the $\mathrm{d}\mathbf{p}$ integral and can be dropped.

5. Fluctuation averages

5.1. Multipole expansion of temperature and polarization correlations in momentum space

The two-point correlation function of the fluctuating temperature field $T_{\mathbf{k}}=T(\omega,\mathbf{k}_0)$ in momentum space (cf. (3.13) and (3.14)) is defined by an angular average [28,29],

$$\langle T(\omega,\mathbf{k}_0)T(\omega,\mathbf{k}'_0)\rangle_\Omega=\frac{1}{8\pi^2}\iint T(\omega,\mathbf{q}_0)T(\omega,\mathbf{q}'_0)\delta(\mathbf{q}_0\mathbf{q}'_0-\mathbf{k}_0\mathbf{k}'_0)\mathrm{d}\Omega_{\mathbf{q}_0}\mathrm{d}\Omega_{\mathbf{q}'_0}, \tag{5.1}$$

which only depends on ω and the polar angle $\mathbf{k}_0\mathbf{k}'_0=\cos\theta$. $\mathrm{d}\Omega_{\mathbf{q}_0}$ and $\mathrm{d}\Omega_{\mathbf{q}'_0}$ are the solid angle elements of $\mathbf{q}_0$ and $\mathbf{q}'_0$ on the unit sphere, and the subscript zero denotes unit vectors. The density $\delta(\mathbf{q}_0\mathbf{q}'_0-\cos\theta)\mathrm{d}\Omega_{\mathbf{q}_0}\mathrm{d}\Omega_{\mathbf{q}'_0}/(8\pi^2)$ in (5.1) is normalized. The polarization autocorrelation $\langle P(\omega,\mathbf{k}_0)P(\omega,\mathbf{k}'_0)\rangle_\Omega$ (with $P(\omega,\mathbf{k}_0)=P_{\mathbf{k}}$, cf. (3.14)), and the cross-correlation $\langle T(\omega,\mathbf{k}_0)P(\omega,\mathbf{k}'_0)\rangle_\Omega$ are defined analogously.

The random fields $T(\omega,\mathbf{k}_0)$ and $P(\omega,\mathbf{k}_0)$ are homogeneous, $\langle T(\omega,\mathbf{k}_0)\rangle_\Omega=\int T(\omega,\mathbf{k}_0)\mathrm{d}\Omega_{\mathbf{k}_0}/(4\pi)=0$ and $\langle P(\omega,\mathbf{k}_0)\rangle_\Omega=0$, since the mean temperature and mean polarization have been split off, cf. (3.13). The isotropic correlation function (5.1) admits an expansion in Legendre polynomials [29],

$$\langle T(\omega,\mathbf{k}_0)T(\omega,\mathbf{k}'_0)\rangle_\Omega=\frac{1}{2\pi}\sum_{l=1}^{\infty}(l+1/2)C_l^{TT}(\omega)P_l(\cos\theta), \tag{5.2}$$

with $\mathbf{k}_0\mathbf{k}'_0=\cos\theta$. The multipole coefficients are calculated from the measured temperature fluctuations as [30]

$$C_l^{TT}(\omega)=\frac{1}{4\pi}\iint T(\omega,\mathbf{k}_0)T(\omega,\mathbf{k}'_0)P_l(\mathbf{k}_0\mathbf{k}'_0)\mathrm{d}\Omega_{\mathbf{k}'_0}\mathrm{d}\Omega_{\mathbf{k}_0}. \tag{5.3}$$

An analogous expansion holds for the polarization correlation $\langle P(\omega,\mathbf{k}_0)P(\omega,\mathbf{k}'_0)\rangle_\Omega$ with multipole coefficients C_l^{PP} and for the cross-correlation $\langle T(\omega,\mathbf{k}_0)P(\omega,\mathbf{k}'_0)\rangle_\Omega$ with coefficients C_l^{TP}. The averaged squares $\langle T^2(\omega,\mathbf{k}_0)\rangle_\Omega$, $\langle P^2(\omega,\mathbf{k}_0)\rangle_\Omega$ and $\langle T(\omega,\mathbf{k}_0)P(\omega,\mathbf{k}_0)\rangle_\Omega$ are independent of the angle $\mathbf{k}_0\mathbf{k}'_0=\cos\theta$, since $P_n(1)=1$ in (5.2).

In the case of the CMB radiation, the temperature and polarization fluctuations $T_{\mathbf{k}}=T(\omega,\mathbf{k}_0)$ and $P_{\mathbf{k}}=P(\omega,\mathbf{k}_0)$ are frequency independent and so are the multipole coefficients C_l^{TT}, $C_l^{PP}\sim C_l^{EE}+C_l^{BB}$ and $C_l^{TP}\sim C_l^{TE}+C_l^{TB}$ which have been measured by the Planck satellite [3]. The indicated decomposition into E and B components stems from the multipole expansion of the Stokes parameters Q and U, with circular polarization V, a pseudoscalar, assumed to be negligible [29]. Here, we only need the scalar combination $P\propto\sqrt{Q^2+U^2+V^2}$ of the Stokes parameters defining the polarization,

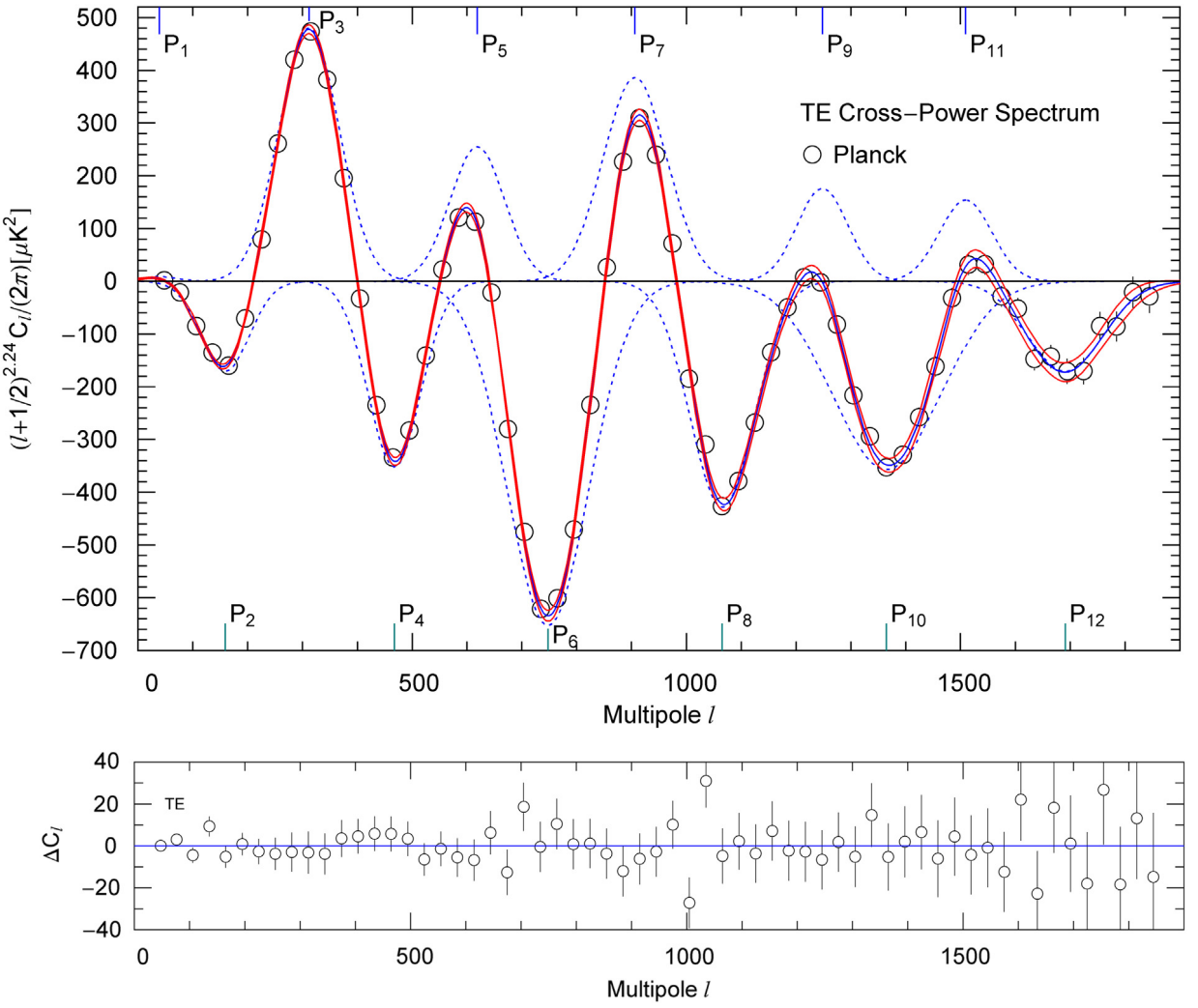

Fig. 1. Temperature-polarization cross-power spectrum of the CMB radiation. Data points (binned) from Ref. [3]. The least-squares fit of the multipole coefficients $C_l^{TP} \sim C_l^{TE}$, cf. after (5.3), is the blue solid curve. The 1σ error band is indicated by the red solid curves, see after (5.5). The fit of the C_l^{TE} is performed with a series of 12 Gaussians (blue dotted curves), rescaled with a power law, $(l+1/2)^{2+\mu}C_l^{TE}/(2\pi) = \sum_{n=1}^{12} a_n \exp[-(l-b_n)^2/(2\sigma_n^2)]$, cf. Section 5.2. The power-law scaling exponent $\mu = 0.24009$ has been obtained from a fit of the temperature power spectrum [30]. The fitting parameters a_n, b_n and σ_n of the Gaussians are recorded in Table 1. The location b_n of the peaks is indicated on the upper and lower abscissae by the approximately equidistant P_n. The residuals of the χ^2 fit are depicted in the lower panel. $\chi^2_{TE}/\mathrm{dof} = 1878.8/1813 = 1.036$.

cf. (3.10). The C_l^{BB} and C_l^{TB} coefficients are also negligible as compared with C_l^{EE} and C_l^{TE}, and the circular polarization coefficients C_l^{VV} and cross-correlation coefficients such as C_l^{TV} have not been measured, so that we will identify $C_l^{PP} \sim C_l^{EE}$ and $C_l^{TP} \sim C_l^{TE}$.

5.2. Gaussian fits to angular power spectra

Analytic representations of the multipole coefficients C_l^{TT}, C_l^{EE} and C_l^{TE} can be obtained from least-squares fits to the measured power spectra, see Figs. 1–4. The fits are performed with a series of Gaussians and an overall power-law scale factor. The temperature multipole coefficients C_l^{TT} can be fitted with eight Gaussians,

$$(l+1/2)^{2+\mu}\frac{C_l^{TT}}{2\pi} = \sum_{n=1}^{8} a_n \exp(-\frac{(l-b_n)^2}{2\sigma_n^2}), \tag{5.4}$$

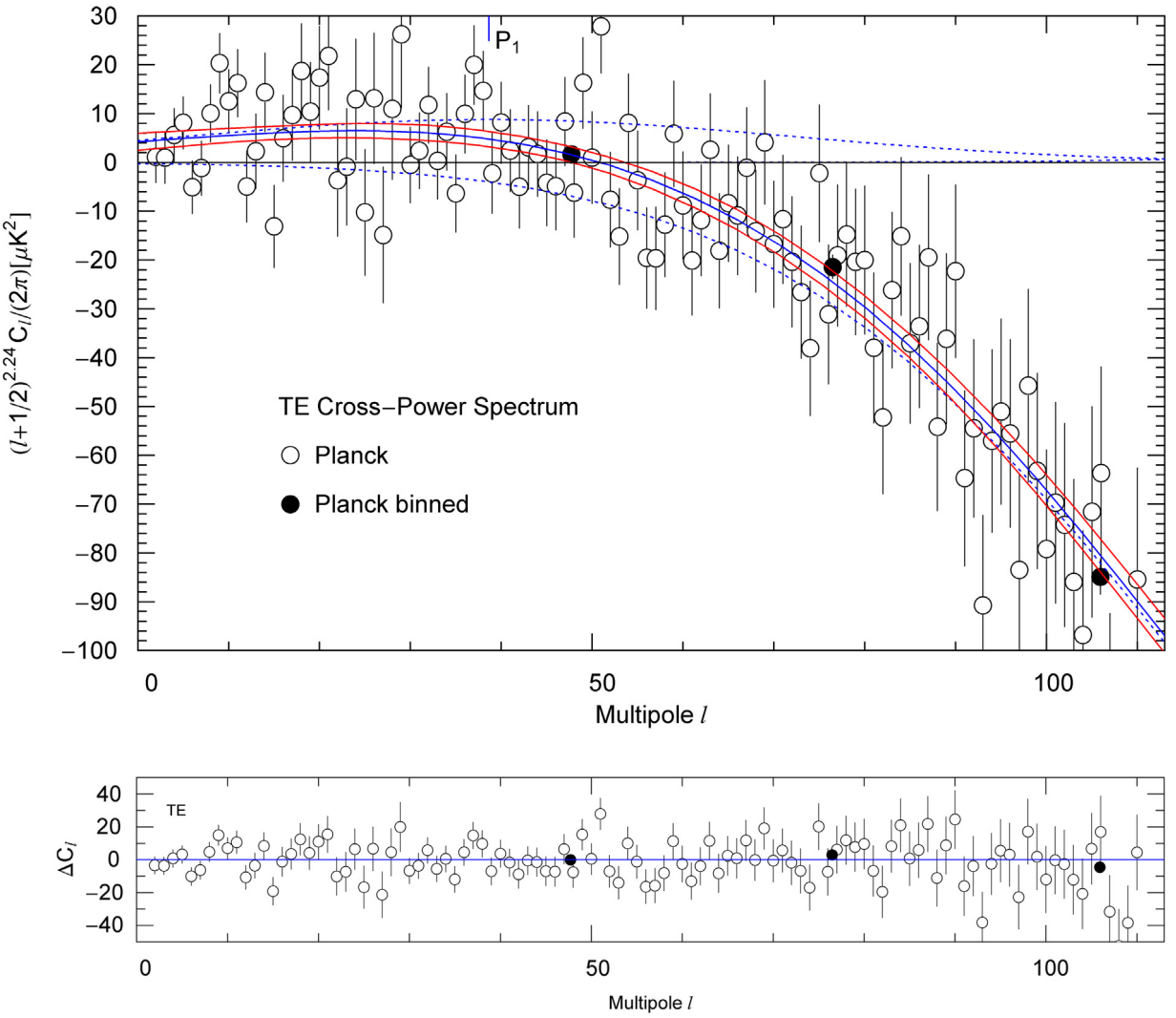

Fig. 2. Close-up of the low-l temperature-polarization cross-power spectrum in Fig. 1 ($2 \le l \le 110$). Data points and notation as in Fig. 1. The filled black circles are the first three binned data points in Fig. 1. The blue solid curve is the χ^2 fit of the multipole coefficients C_l^{TE}, the 1σ error band is depicted in red, cf. Section 5.2. Despite the large spread of the data points at low l, the error band defined by the least-squares fit (5.5) is quite narrow. The blue dotted curves indicate the first two Gaussians in Fig. 1; the subsequent peaks do not contribute in this l range. Residuals are shown in the lower panel.

and the C_l^{EE} and C_l^{TE} spectra are fitted with six and twelve Gaussians, respectively. The power-law exponent μ and the parameters a_n, b_n, σ_n defining the Gaussians are inferred from the spectral fits, cf. Table 1.

We briefly explain the fits and the error bands depicted in the figures. The fit of the temperature multipoles C_l^{TT} is based on the least-squares functional

$$\chi^2_{TT}(\mu,(a_n,b_n,\sigma_n)_{n=1,\dots,8}) = \sum_{l=2}^{2508}\Big(\frac{C_l^{TT}(\mu,(a_n,b_n,\sigma_n)_{n=1,\dots,8}) - C^{TT}_{\mathrm{exp},l}}{\sigma^{TT}_{\mathrm{exp},l}}\Big)^2. \tag{5.5}$$

Here, the $C^{TT}_{\mathrm{exp},l}$, $l = 2,\dots,2508$, denote the measured multipole coefficients, and the $\sigma^{TT}_{\mathrm{exp},l}$ are the corresponding error estimates for each $C^{TT}_{\mathrm{exp},l}$ (statistical and systematic, added in square) as recorded in Ref. [3]. $C_l^{TT}(\mu,(a_n,b_n,\sigma_n)_{n=1,\dots,8})$ is the analytic fit function in (5.4). The chi-square functional χ^2_{TT} in (5.5) attains its minimum at the parameter values μ and a_n, b_n, σ_n, $n = 1,\dots,8$, listed in Table 1.

The least-squares fits of the polarization power spectra C_l^{TE} and C_l^{EE} are performed analogously, with chi-square functionals defined as in (5.5): $\chi^2_{TE}((a_n,b_n,\sigma_n)_{n=1,\dots,12})$ (summed over $2 \le l \le 1850$ measured multipoles) and

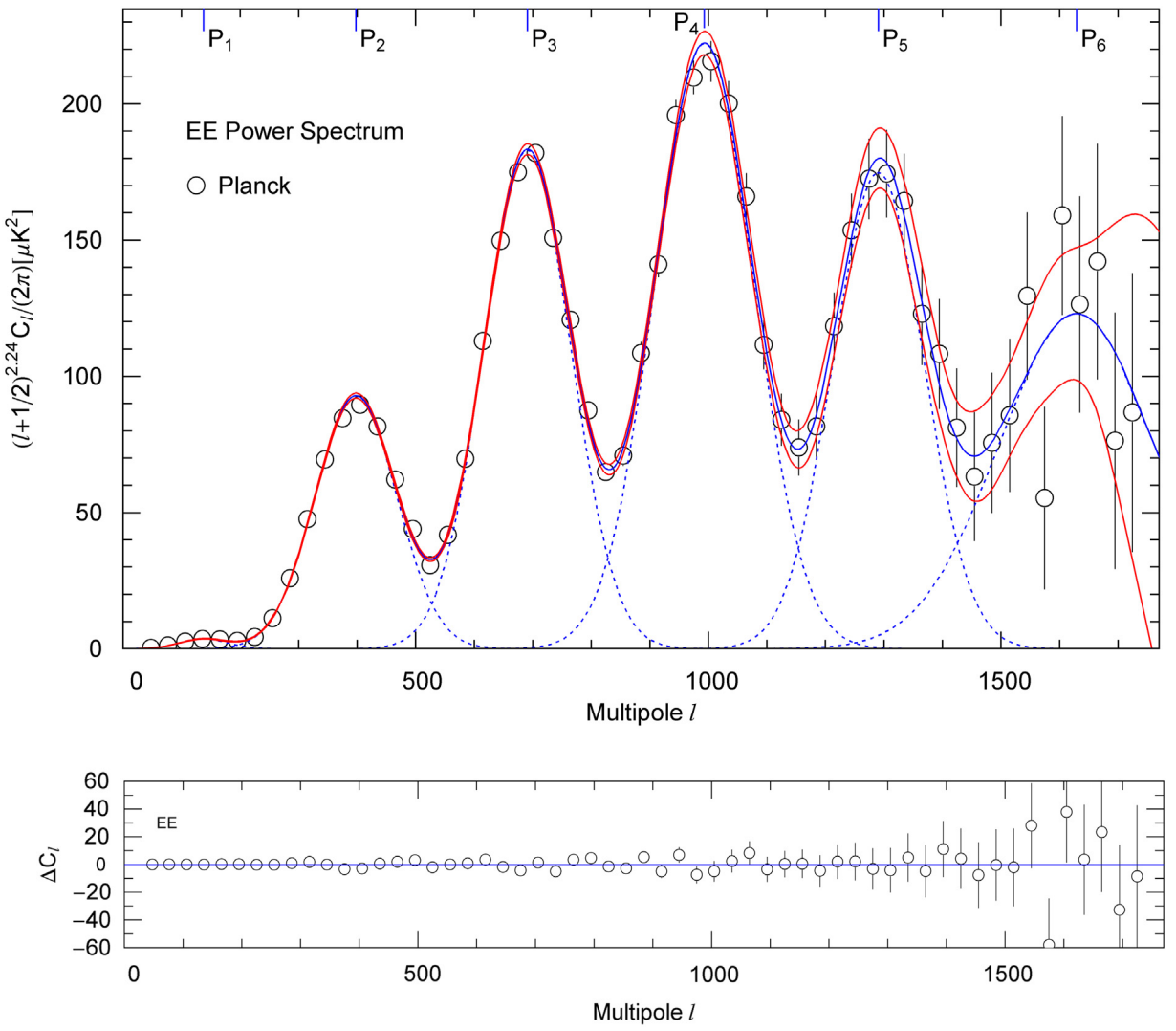

Fig. 3. Polarization power spectrum of the CMB radiation. Data points (binned) from Ref. [3]. The least-squares fit of the multipole coefficients $C_l^{PP} \sim C_l^{EE}$ (see after (5.3)) is the blue solid curve. The 1σ error band is indicated by the red solid curves. The fit of the C_l^{EE} coefficients is performed with a series of six Gaussians, $(l+1/2)^{2+\mu}C_l^{EE}/(2\pi) = \sum_{n=1}^{6} a_n \exp[-(l-b_n)^2/(2\sigma_n^2)]$ (blue dotted curves), see the caption to Fig. 1 and Section 5.2. The fit parameters defining the Gaussians are listed in Table 1. The peaks of the Gaussians are indicated on the upper abscissa by the nearly equidistant P_n. The residuals of the χ^2 fit are depicted in the lower panel. $\chi^2_{EE}/\text{dof} = 1745.9/1681 = 1.039$.

$\chi^2_{EE}((a_n, b_n, \sigma_n)_{n=1,\ldots,6})$ (with $2 \le l \le 1700$ multipoles); the power-law exponent μ is taken as input from the fit of the temperature spectrum C_l^{TT}. The minimization of the chi-square functionals is numerically readily done, since the data points quite accurately define Gaussian peaks, so that a good initial guess of the parameters (a_n, b_n, σ_n) of the Gaussians in (5.4) can easily be found, the more so as the Gaussians only weakly overlap and thus only slightly affect the initial guesses for the neighboring peaks.

To obtain the error band, we rename the fitting parameters μ and a_n, b_n, σ_n in (5.5) as y_k, $k = 0, \ldots, 24$, (e.g., $y_0 = \mu$, $y_{3n-2} = a_n$, $y_{3n-1} = b_n$, $y_{3n} = \sigma_n$, $n = 1, \ldots, 8$) and denote the 25×25 matrix of the second-order derivatives of $\chi^2(y_k)$ in (5.5) by $H_{ij} = (1/2)\partial^2\chi^2/\partial y_i \partial y_j$, $i, j = 0, \ldots, 24$. The factor of one-half in front of the Hessian stems from the Taylor expansion of the chi-square functional around the minimum y_k; the gradient $\partial\chi^2/\partial y_i$ vanishes at this stationary point. (In the case of the χ^2_{TE} and χ^2_{EE} functionals, the index range of the Hessian is $i, j = 1, \ldots, 36$ and $i, j = 1, \ldots, 18$, respectively.)

The inverse of H_{ij} defines the covariance matrix, $\text{cov}_{ij} = H^{-1}_{ij}$; the variances of the variables y_k (which minimize χ^2) are the diagonal elements $\sigma_k^2 = \text{cov}_{kk}$. Returning to the analytic representation of the multipole coefficients $C_l(y_k)$ in (5.4), we calculate the gradient $G_{l,i} = \partial C_l/\partial y_i$, $i = 0, \ldots, 24$, at the stationary point y_k of χ^2. The variance of the fit function $C_l(y_k)$ is then obtained, for each multipole index l, as $\sigma_l^2 = \sum_{i,j=0}^{24} G_{l,i}\text{cov}_{ij}G_{l,j}$, evaluated at y_k. The standard deviations σ_l define the 1σ error band $C_l \pm \sigma_l$ depicted in Figs. 1–4. (The multipole index l is integer, but the fit function C_l in (5.4)

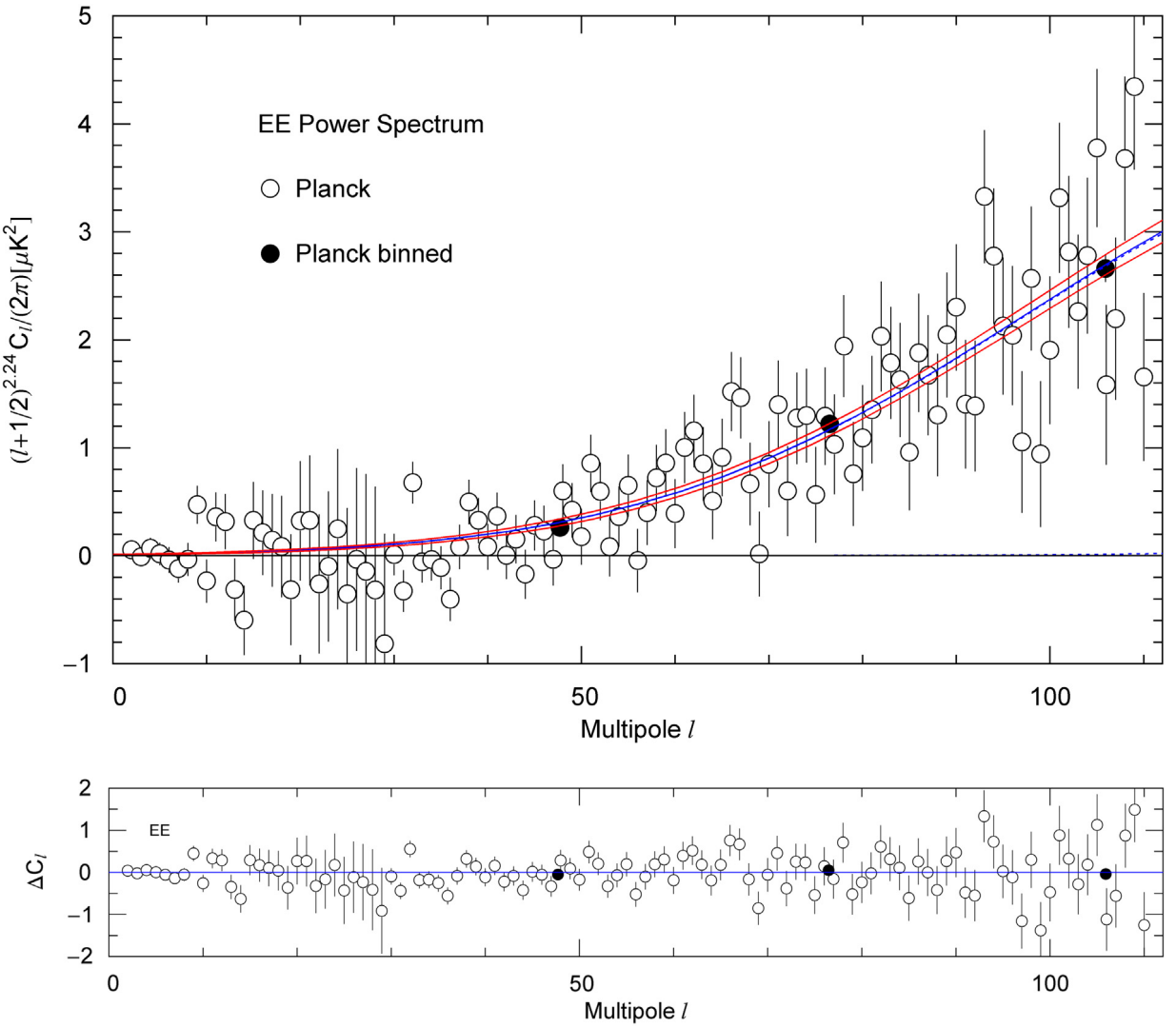

Fig. 4. Close-up of the low-l polarization power spectrum in Fig. 3, covering the multipole range $2 \le l \le 110$. Data points as in Fig. 3. The filled black circles are the first three binned data points in Fig. 3. The solid blue curve is the χ^2 fit of the multipole coefficients C_l^{EE}, cf. Section 5.2, the 1σ error band is depicted in red. Despite the large error bars of the data points, the error band is narrow, also compare to Fig. 2. The fit in this multipole range is indistinguishable from the first Gaussian in Fig. 3. The residuals are depicted in the lower panel.

and the σ_l are smooth functions for real l.) The experimental error bars in Figs. 2 and 4 are large at low multipoles, but the fluctuations in the data sets average out, as indicated by the narrow error bands at low l. Therefore, the multipole coefficients can be obtained from the analytic fits with good precision σ_l, despite the large error bars of the low-l data sets.

5.3. Angular fluctuation average of the polarized and unpolarized intensity components

The fluctuation expansion of the unpolarized and polarized intensity components $I_{\text{unpol}} = 2\rho_{2,\mathbf{k}}$ and $I_{\text{totpol}} = \rho_{1,\mathbf{k}} - \rho_{2,\mathbf{k}}$ in (3.20) is stated in (3.17) and (3.18). The angular average thereof is performed as in (5.1),

$$\begin{aligned}\langle I_{\text{unpol}}\rangle_\Omega &= 2\rho^{\text{iso}} - 2\rho^{\text{iso}}_{,T_0}P_0 + \rho^{\text{iso}}_{,T_0,T_0}(\langle T_{\mathbf{k}}^2\rangle_\Omega + P_0^2 + \langle P_{\mathbf{k}}^2\rangle_\Omega - 2\langle T_{\mathbf{k}}P_{\mathbf{k}}\rangle_\Omega),\\ \langle I_{\text{totpol}}\rangle_\Omega &= 2\rho^{\text{iso}}_{,T_0}P_0 + 2\rho^{\text{iso}}_{,T_0,T_0}\langle T_{\mathbf{k}}P_{\mathbf{k}}\rangle_\Omega,\end{aligned} \tag{5.6}$$

Table 1
Fitting parameters of the multipole coefficients C_l^{TT}, C_l^{TE} and C_l^{EE} of the CMB temperature autocorrelation, the temperature-polarization cross-correlation and the polarization autocorrelation, respectively, see Section 5.2. The χ^2 fits are performed with a series of Gaussians rescaled with a power law, $(l+1/2)^{2+\mu}C_l/(2\pi) = \sum_n a_n \exp[-(l-b_n)^2/(2\sigma_n^2)]$, see after (5.4) and the captions to Figs. 1 and 3. The power-law exponent $\mu = 0.24009$ has been obtained from a fit of the temperature power spectrum [30]. Recorded are the amplitudes a_n, peaks b_n and RMS widths σ_n of the Gaussians. The C_l^{TE} and C_l^{EE} power spectra are shown in Figs. 1–4; the fit of the temperature autocorrelation coefficients C_l^{TT} is depicted in Figs. 1 and 2 of Ref. [30].

n	$a_n^{TT}[\mu K^2]$	b_n^{TT}	σ_n^{TT}	$a_n^{TE}[\mu K^2]$	b_n^{TE}	σ_n^{TE}	$a_n^{EE}[\mu K^2]$	b_n^{EE}	σ_n^{EE}
1	21015.	227.38	93.426	8.8007	38.646	33.299	3.6536	137.77	40.547
2	11276.	536.28	90.761	−170.06	158.94	43.896	92.840	397.80	69.590
3	12474.	818.60	107.11	480.29	311.77	54.615	182.98	690.70	74.397
4	6258.0	1130.1	98.473	−351.45	467.32	47.819	222.17	993.19	84.302
5	4530.1	1426.7	123.24	254.92	618.61	49.737	174.67	1290.4	77.453
6	1993.0	1741.6	105.28	−652.36	747.63	74.252	122.98	1629.2	133.47
7	1378.0	2034.3	148.28	386.35	906.20	58.222	-	-	-
8	615.01	2390.9	113.98	−428.23	1065.2	57.880	-	-	-
9	-	-	-	176.00	1248.2	46.360	-	-	-
10	-	-	-	−356.98	1365.0	97.899	-	-	-
11	-	-	-	153.95	1509.3	47.796	-	-	-
12	-	-	-	−170.78	1691.1	68.688	-	-	-

where $\rho^{\rm iso}(\omega)$ is the isotropic spectral density in (3.16). The averaged quantities in (5.6) are independent of the wave vector and read (cf. (5.2) and after (5.3)),

$$\langle T_{\mathbf{k}}^2\rangle_\Omega = \frac{1}{2\pi}\sum_{l=1}^\infty (l+1/2)C_l^{TT}, \quad \langle T_{\mathbf{k}}P_{\mathbf{k}}\rangle_\Omega = \frac{1}{2\pi}\sum_{l=1}^\infty (l+1/2)C_l^{TP},$$
$$P_0^2 + \langle P_{\mathbf{k}}^2\rangle_\Omega = \frac{1}{2\pi}\sum_{l=0}^\infty (l+1/2)C_l^{PP}, \quad P_0 = \sqrt{C_0^{PP}/(4\pi)}. \tag{5.7}$$

As for the microwave background radiation, we find $\langle T_{\mathbf{k}}^2\rangle_\Omega/T_0^2 = 1.770\times 10^{-9}$, $\langle T_{\mathbf{k}}P_{\mathbf{k}}\rangle_\Omega/T_0^2 = -2.791\times 10^{-12}$ and $(P_0^2+\langle P_{\mathbf{k}}^2\rangle_\Omega)/T_0^2 = 5.348\times 10^{-12}$, as well as $P_0/T_0 = 6.016\times 10^{-8}$, where $T_0 = 2.7255$ K [31] is the CMB mean temperature, cf. (3.14). These estimates are obtained by substituting the Gaussian spectral fits (5.4) for the multipole coefficients in (5.7). (The analytic fits admit a narrow error band at low multipoles, despite the large spread of the data points, see. Figs. 2 and 4. Therefore, we use the Gaussian fits (5.4) rather than the measured multipole coefficients in series (5.7).) The angular temperature and polarization fluctuations relative to the mean temperature are $\Delta T/T_0 = 4.21\times 10^{-5}$ and $\Delta P/T_0 = 2.31\times 10^{-6}$, with $\Delta T = \sqrt{\langle T_{\mathbf{k}}^2\rangle_\Omega}$ and $\Delta P = \sqrt{P_0^2+\langle P_{\mathbf{k}}^2\rangle_\Omega}$. That is, the CMB polarization fluctuations are by one order smaller than the temperature fluctuations.

The fluctuation-averaged total intensity is $\langle I\rangle_\Omega = \langle I_{\rm unpol}\rangle_\Omega + \langle I_{\rm totpol}\rangle_\Omega$, cf. (5.6), and the frequency-dependent polarization degree is $\langle I_{\rm totpol}\rangle_\Omega/\langle I\rangle_\Omega$. The spectral peak of the isotropic Planckian density $\rho^{\rm iso}(\omega)$ in (3.16) is located at $\omega_{\max}/T_0 \sim 2.8214$ where $T_0\rho^{\rm iso}_{,T_0}/\rho^{\rm iso} = 3$, so that $\langle I_{\rm totpol}\rangle_\Omega/\langle I\rangle_\Omega \sim 3P_0/T_0 = 1.80\times 10^{-7}$ at the peak frequency $\omega_{\max}$, cf. (5.6).

The specific internal energy of the unpolarized radiation component is $U_{\rm unpol}/V = 4\pi\int_0^\infty \langle I_{\rm unpol}\rangle_\Omega {\rm d}\omega$, cf. (2.11), and analogously for the energy $U_{\rm totpol}/V$ of the totally polarized component $\langle I_{\rm totpol}\rangle$. The frequency integration of the expansions (5.6) gives

$$\frac{U_{\rm unpol}}{V} = \frac{\pi^2}{15}T_0^4[1-4\frac{P_0}{T_0}+\frac{6}{T_0^2}(\langle T_{\mathbf{k}}^2\rangle_\Omega + P_0^2 + \langle P_{\mathbf{k}}^2\rangle_\Omega - 2\langle T_{\mathbf{k}}P_{\mathbf{k}}\rangle_\Omega)],$$
$$\frac{U_{\rm totpol}}{V} = \frac{4\pi^2}{15}T_0^4(\frac{P_0}{T_0}+3\frac{\langle T_{\mathbf{k}}P_{\mathbf{k}}\rangle_\Omega}{T_0^2}), \tag{5.8}$$

where we substitute the estimates stated after (5.7). The total internal energy is $U = U_{\rm unpol}+U_{\rm totpol}$. Only a small fraction of the CMB radiation is polarized, $U_{\rm totpol}/U \sim 4P_0/T_0 \sim 2.406\times 10^{-7}$.

5.4. Energy density correlations induced by temperature and polarization fluctuations

We isotropize the energy density correlation (4.9) by performing a fluctuation average (denoted by angle brackets with a subscript Ω) as in (5.1),

$$\langle\langle \Delta\mathbf{E}^2(\mathbf{x},t)\Delta\mathbf{E}^2(\mathbf{y},t)\rangle\rangle_\Omega = \int {\rm e}^{-{\rm i}\mathbf{k}(\mathbf{x}-\mathbf{y})}{\rm e}^{{\rm i}\mathbf{p}(\mathbf{x}-\mathbf{y})}\langle\rho_{1,\mathbf{k}}\rho_{1,\mathbf{p}}+\rho_{2,\mathbf{k}}\rho_{2,\mathbf{p}}\rangle_\Omega {\rm d}\omega_{\mathbf{k}}{\rm d}\Omega_{\mathbf{k}_0}{\rm d}\omega_{\mathbf{p}}{\rm d}\Omega_{\mathbf{p}_0}$$
$$+\frac{1}{(2\pi)^3}\int \omega_{\mathbf{p}}{\rm e}^{{\rm i}\mathbf{p}(\mathbf{x}-\mathbf{y})}{\rm d}\mathbf{p}\int {\rm e}^{-{\rm i}\mathbf{k}(\mathbf{x}-\mathbf{y})}\langle\rho_{1,\mathbf{k}}+\rho_{2,\mathbf{k}}\rangle_\Omega {\rm d}\omega_{\mathbf{k}}{\rm d}\Omega_{\mathbf{k}_0}. \tag{5.9}$$

Here, we use the shortcut $\rho_{j,\mathbf{k}} = \rho_j(\omega, \mathbf{k}_0)$ for the spectral density in (2.11) and (4.9), and expand this density in the temperature and polarization fluctuations as done in (3.17),

$$\langle \rho_{1,\mathbf{k}}\rho_{1,\mathbf{p}} + \rho_{2,\mathbf{k}}\rho_{2,\mathbf{p}}\rangle_\Omega = 2\rho^{\rm iso}_{\mathbf{k}}\rho^{\rm iso}_{\mathbf{p}} + \rho^{\rm iso}_{\mathbf{p}}\rho^{\rm iso}_{\mathbf{k},T_0,T_0}(\langle T^2_{\mathbf{k}}\rangle_\Omega + P_0^2 + \langle P^2_{\mathbf{k}}\rangle_\Omega)$$
$$+\rho^{\rm iso}_{\mathbf{k}}\rho^{\rm iso}_{\mathbf{p},T_0,T_0}(\langle T^2_{\mathbf{p}}\rangle_\Omega + P_0^2 + \langle P^2_{\mathbf{p}}\rangle_\Omega) + 2\rho^{\rm iso}_{\mathbf{k},T_0}\rho^{\rm iso}_{\mathbf{p},T_0}(\langle T_{\mathbf{k}}T_{\mathbf{p}}\rangle_\Omega + P_0^2 + \langle P_{\mathbf{k}}P_{\mathbf{p}}\rangle_\Omega). \tag{5.10}$$

(The linear terms vanish because of $\langle T_{\mathbf{k}}\rangle_\Omega = \langle P_{\mathbf{k}}\rangle_\Omega = 0$, cf. (3.13) and (3.14).) $\rho^{\rm iso}_{\mathbf{k}}$ is the isotropic spectral density in (3.16), with $\omega = k$. The expectation values $\langle T_{\mathbf{k}}T_{\mathbf{p}}\rangle_\Omega = \langle T(\omega,\mathbf{k}_0)T(\omega,\mathbf{p}_0)\rangle_\Omega$ and $\langle P_{\mathbf{k}}P_{\mathbf{p}}\rangle_\Omega$ are defined by the multipole series in (5.2), and the constants $\langle T^2_{\mathbf{k}}\rangle_\Omega$ and $P_0^2 + \langle P^2_{\mathbf{k}}\rangle_\Omega$ are stated in (5.7). The analogous second-order expansion of the average $\langle \rho_{1,\mathbf{k}} + \rho_{2,\mathbf{k}}\rangle_\Omega$ in (5.9) is

$$\langle \rho_{1,\mathbf{k}} + \rho_{2,\mathbf{k}}\rangle_\Omega = 2\rho^{\rm iso}_{\mathbf{k}} + \rho^{\rm iso}_{\mathbf{k},T_0,T_0}(\langle T^2_{\mathbf{k}}\rangle_\Omega + P_0^2 + \langle P^2_{\mathbf{k}}\rangle_\Omega). \tag{5.11}$$

Substituting these expansions into (5.9), we obtain

$$\langle\langle \Delta\mathbf{E}^2(\mathbf{x},t)\Delta\mathbf{E}^2(\mathbf{y},t)\rangle\rangle_\Omega = G_{\rm iso} + G_T + G_P + G_{\rm sing}, \tag{5.12}$$

where $G_{\rm iso}$ is the isotropic correlation function of an ideal photon gas at T_0,

$$G_{\rm iso} = 2\int \mathrm{e}^{-\mathrm{i}\mathbf{k}(\mathbf{x}-\mathbf{y})}\rho^{\rm iso}_{\mathbf{k}}\mathrm{d}\omega_{\mathbf{k}}\mathrm{d}\Omega_{\mathbf{k}_0}\int \mathrm{e}^{\mathrm{i}\mathbf{p}(\mathbf{x}-\mathbf{y})}\rho^{\rm iso}_{\mathbf{p}}\mathrm{d}\omega_{\mathbf{p}}\mathrm{d}\Omega_{\mathbf{p}_0}. \tag{5.13}$$

The correlation generated by the temperature fluctuations is $G_T = G_{T1} + G_{T2}$, where

$$G_{T1} = 2\int \mathrm{e}^{\mathrm{i}\mathbf{p}(\mathbf{x}-\mathbf{y})}\rho^{\rm iso}_{\mathbf{p}}\mathrm{d}\omega_{\mathbf{p}}\mathrm{d}\Omega_{\mathbf{p}_0}\int \mathrm{e}^{-\mathrm{i}\mathbf{k}(\mathbf{x}-\mathbf{y})}\rho^{\rm iso}_{\mathbf{k},T_0,T_0}\langle T^2_{\mathbf{k}}\rangle_\Omega\mathrm{d}\omega_{\mathbf{k}}\mathrm{d}\Omega_{\mathbf{k}_0},$$
$$G_{T2} = 2\int \mathrm{e}^{-\mathrm{i}\mathbf{k}(\mathbf{x}-\mathbf{y})}\mathrm{e}^{\mathrm{i}\mathbf{p}(\mathbf{x}-\mathbf{y})}\rho^{\rm iso}_{\mathbf{k},T_0}\rho^{\rm iso}_{\mathbf{p},T_0}\langle T_{\mathbf{k}}T_{\mathbf{p}}\rangle_\Omega\mathrm{d}\omega_{\mathbf{k}}\mathrm{d}\Omega_{\mathbf{k}_0}\mathrm{d}\omega_{\mathbf{p}}\mathrm{d}\Omega_{\mathbf{p}_0}. \tag{5.14}$$

The correlation induced by polarization is $G_P = G_{P1} + G_{P2}$, where

$$G_{P1} = 2\int \mathrm{e}^{\mathrm{i}\mathbf{p}(\mathbf{x}-\mathbf{y})}\rho^{\rm iso}_{\mathbf{p}}\mathrm{d}\omega_{\mathbf{p}}\mathrm{d}\Omega_{\mathbf{p}_0}\int \mathrm{e}^{-\mathrm{i}\mathbf{k}(\mathbf{x}-\mathbf{y})}\rho^{\rm iso}_{\mathbf{k},T_0,T_0}(P_0^2 + \langle P^2_{\mathbf{k}}\rangle_\Omega)\mathrm{d}\omega_{\mathbf{k}}\mathrm{d}\Omega_{\mathbf{k}_0}$$
$$G_{P2} = 2\int \mathrm{e}^{-\mathrm{i}\mathbf{k}(\mathbf{x}-\mathbf{y})}\mathrm{e}^{\mathrm{i}\mathbf{p}(\mathbf{x}-\mathbf{y})}\rho^{\rm iso}_{\mathbf{k},T_0}\rho^{\rm iso}_{\mathbf{p},T_0}(P_0^2 + \langle P_{\mathbf{k}}P_{\mathbf{p}}\rangle_\Omega)\mathrm{d}\omega_{\mathbf{k}}\mathrm{d}\Omega_{\mathbf{k}_0}\mathrm{d}\omega_{\mathbf{p}}\mathrm{d}\Omega_{\mathbf{p}_0}. \tag{5.15}$$

The singular term $G_{\rm sing}$ in (5.12) is the zero-point divergence, cf. after (4.9),

$$G_{\rm sing} = 2\int \mathrm{e}^{-\mathrm{i}\mathbf{k}(\mathbf{x}-\mathbf{y})}[\rho^{\rm iso}_{\mathbf{k}} + \frac{1}{2}\rho^{\rm iso}_{\mathbf{k},T_0,T_0}(\langle T^2_{\mathbf{k}}\rangle_\Omega + P_0^2 + \langle P^2_{\mathbf{k}}\rangle_\Omega)]\mathrm{d}\omega_{\mathbf{k}}\mathrm{d}\Omega_{\mathbf{k}_0}$$
$$\times\frac{1}{(2\pi)^3}\int \omega_{\mathbf{p}}\mathrm{e}^{\mathrm{i}\mathbf{p}(\mathbf{x}-\mathbf{y})}\mathrm{d}\mathbf{p}. \tag{5.16}$$

In the following, we will drop this divergent term in (5.12) and regard $G(r) = G_{\rm iso} + G_T + G_P$ as proper energy density correlation function, which is finite at $r = 0$.

6. Spectral representation of fluctuation-averaged energy density correlations

The angular integration of the isotropic correlation $G_{\rm iso}$ in (5.12) and (5.13), by way of $\int \mathrm{e}^{\pm\mathrm{i}\mathbf{k}\mathbf{x}}\mathrm{d}\Omega_{\mathbf{k}_0} = 4\pi\,\sin(kr)/(kr)$, gives the isotropic spectral kernel $g_{\rm iso}(r;\omega,\omega')$, $r = |\mathbf{x}-\mathbf{y}|$,

$$G_{\rm iso}(r) = \int_0^\infty g_{\rm iso}(r;\omega,\omega')\mathrm{d}\omega\mathrm{d}\omega', \tag{6.1}$$

$$g_{\rm iso}(r;\omega,\omega') = 2\frac{(4\pi)^2}{(2\pi)^6}\frac{\omega^2}{\mathrm{e}^{\omega/T_0}-1}\frac{\omega'^2}{\mathrm{e}^{\omega'/T_0}-1}\frac{1}{r^2}\sin(\omega r)\sin(\omega' r). \tag{6.2}$$

The spectral representation of the correlation induced by temperature fluctuations, $G_T(r) = G_{T1} + G_{T2}$ in (5.14), and the correlation induced by polarization, $G_P(r) = G_{P1} + G_{P2}$ in (5.15), is defined analogously by

$$G_{T1,T2,P1,P2}(r) = \int_0^\infty g_{T1,T2,P1,P2}(r;\omega,\omega')\mathrm{d}\omega\mathrm{d}\omega'. \tag{6.3}$$

The kernel $g_{T1}(r;\omega,\omega')$ of $G_{T1}(r)$ reads

$$g_{T1}(r;\omega,\omega') = 2\frac{(4\pi)^2}{(2\pi)^6}\langle T^2_{\mathbf{k}}\rangle_\Omega\frac{1}{2}[\frac{\omega'^2}{\mathrm{e}^{\omega'/T_0}-1}(\frac{\omega^2}{\mathrm{e}^{\omega/T_0}-1})_{,T_0,T_0}$$
$$+(\omega\leftrightarrow\omega')]\frac{1}{r^2}\sin(\omega r)\sin(\omega' r) \tag{6.4}$$

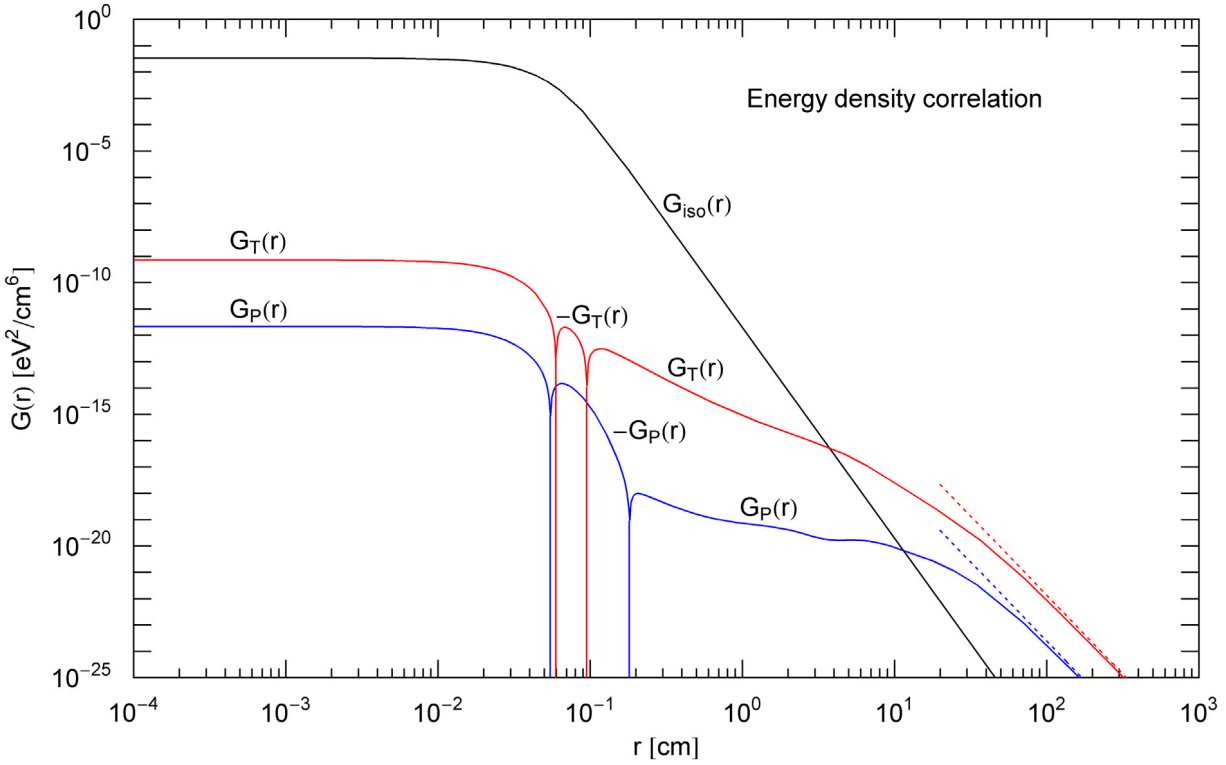

Fig. 5. Energy density autocorrelations of the CMB radiation. $G_{\rm iso}(r)$ (black curve) is the isotropic correlation of an ideal photon gas defined by the mean temperature, cf. (6.1). The temperature fluctuations generate the correlation $G_T(r)$ (red curve), and the polarization fluctuations the correlation $G_P(r)$ (blue curve), cf. (6.3). All three correlations are long-range: $G_{\rm iso}(r)$ decays $\propto 1/r^8$ at large distance, whereas $G_T(r)$ and $G_P(r)$ decay $\propto 1/r^6$ (dotted lines) and overpower the isotropic correlation. At short distance, $r \leq 0.01$ cm, the correlations are nearly constant. In the crossover regime, the correlations $G_{T,P}(r)$ become negative and are depicted as $-G_{T,P}(r)$ in this double-logarithmic plot.

where the temperature average $\langle T^2_{\mathbf{k}}\rangle_\Omega$ is a constant defined by the multipole series in (5.7). The kernel $g_{P1}(r;\omega,\omega')$ of the polarization correlation $G_{P1}(r)$ is obtained by replacing $\langle T^2_{\mathbf{k}}\rangle_\Omega$ in (6.4) by the polarization average $P_0^2+\langle P^2_{\mathbf{k}}\rangle_\Omega$, which is also a constant calculated in (5.7).

To perform the angular integrations defining the correlations $G_{T2,P2}(r)$ in (5.14) and (5.15), we use the integral representation [32,33]

$$\int P_n(\mathbf{k}_0\mathbf{p}_0)\mathrm{e}^{\mathrm{i}\mathbf{k}\mathbf{x}}\mathrm{d}\Omega_{\mathbf{k}_0}\mathrm{e}^{-\mathrm{i}\mathbf{p}\mathbf{x}}\mathrm{d}\Omega_{\mathbf{p}_0}=(4\pi)^2 j_n(kr)j_n(pr), \tag{6.5}$$

where P_n is a Legendre polynomial and the j_n are spherical Bessel functions. The same spherical Fourier integration of the Legendre series of the temperature correlation in (5.2) gives

$$\int \langle T_{\mathbf{k}}T_{\mathbf{p}}\rangle_\Omega \mathrm{e}^{\mathrm{i}\mathbf{k}\mathbf{x}}\mathrm{d}\Omega_{\mathbf{k}_0}\mathrm{e}^{-\mathrm{i}\mathbf{p}\mathbf{x}}\mathrm{d}\Omega_{\mathbf{p}_0}=\frac{(4\pi)^2}{2\pi}\sum_{l=1}^{\infty}(l+1/2)C_l^{TT}j_l(kr)j_l(pr). \tag{6.6}$$

In this way, we find the spectral kernel of correlation $G_{T2}(r)$ in (5.14),

$$g_{T2}(r;\omega,\omega')=2\frac{(4\pi)^2}{(2\pi)^6}\Big(\frac{\omega^3}{\mathrm{e}^{\omega/T_0}-1}\Big)_{,T_0}\Big(\frac{\omega'^3}{\mathrm{e}^{\omega'/T_0}-1}\Big)_{,T_0}$$
$$\times\ \frac{1}{2\pi}\sum_{l=1}^{\infty}(l+1/2)C_l^{TT}j_l(\omega r)j_l(\omega' r). \tag{6.7}$$

The spectral kernel $g_{P2}(r;\omega,\omega')$ of the polarization-induced correlation $G_{P2}(r)$ in (5.15) is obtained by replacing the multipole coefficients C_l^{TT} in (6.7) by the coefficients C_l^{PP} of the polarization correlation $\langle P_{\mathbf{k}}P_{\mathbf{p}}\rangle_\Omega$, cf. after (5.3). In this case, the summation in (6.7) starts with the monopole $l=0$, to accommodate the P_0^2 term in (5.15), cf. (5.7). The Gaussian representation of the multipole coefficients stated in (5.4) and in the caption of Table 1 is substituted in series (6.7). The frequency integrations of the spectral kernels in (6.1) and (6.3) factorize (after interchange of summation and integration). The integration of the kernels $g_{\rm iso}(r;\omega,\omega')$ and $g_{T1,P1}(r;\omega,\omega')$ in (6.1) and (6.4) can be done in closed form with the

Hurwitz zeta function [34]. The factorized integrals of the kernels $g_{T2,P2}(r;\omega,\omega')$ defined by the Neumann series (6.7) can efficiently be calculated by employing the Airy approximation of high-index Bessel functions [35]. Fig. 5 shows the isotropic correlation $G_{\rm iso}(r)$ of ideal (isotropic, unpolarized) black-body radiation at the CMB mean temperature T_0, cf. (6.1). Also depicted are the isotropized CMB correlations $G_T(r)=G_{T1}+G_{T2}$ and $G_P(r)=G_{P1}+G_{P2}$ generated by angular temperature and polarization fluctuations, cf. (6.3), their asymptotic limit and crossover extending over several decades in distance.

7. Conclusion

Ideal black-body radiation is unpolarized and isotropic. In Section 2, we derived the spectral density of a photon gas which is partially polarized and anisotropic. To this end, we used a statistical operator with independent temperature variables for radiation modes in two freely chosen orthogonal polarization states. In Section 3, we obtained the polarization matrix by way of a unitary transformation of the annihilation and creation operators and parametrized this transformation and the temperature variables of the statistical operator by Stokes parameters. In the case of anisotropy, the Stokes parameters depend on the photonic wave vector. The spectral intensity admits an unambiguous decomposition into an unpolarized and a totally polarized radiation component.

In Section 4, we derived spatial correlation functions of the electric field strength in a polarized anisotropic photon gas, at first two-point correlations and then a special case of four-point functions defining energy density correlations. Up to this point, there are no approximations involved, no particular assumptions regarding the frequency and angular-dependent Stokes parameters or the smallness of the polarization degree. The polarized radiation component can be elliptically polarized, including the linear and circular limit cases.

In Sections 5 and 6, we have put the formalism developed to test by applying it to the cosmic microwave background (CMB) radiation, using precision measurements of the CMB temperature anisotropy and polarization. Thermodynamic conversion processes of polarized black-body radiation, especially with regard to solar energy applications, have been studied in Refs. [36,37].

The CMB angular temperature and polarization fluctuations are very small relative to the mean temperature, of order 10^{-5} and 10^{-6} respectively, see Section 5.3. Therefore, one can expand the spectral densities and spatial energy density correlations in the temperature and polarization fluctuations. Subsequently, one performs an angular average of the fluctuation fields, cf. Section 5.1, which results in isotropic quantities, that is angular-independent intensities, cf. Section 5.3, and energy density correlations depending only on distance, cf. Section 6.

The energy density autocorrelation $G(r)=G_{\rm iso}+G_T+G_P$ consists of the isotropic correlation $G_{\rm iso}(r)$ (of an ideal photon gas defined by the mean temperature) and two isotropized correlations $G_{T,P}(r)$ generated by temperature and polarization fluctuations. For the CMB radiation, these correlations are depicted in Fig. 5. All three correlations are nearly constant at short distance and admit long-range power-law decay. At large distance, the isotropic component $G_{\rm iso}(r)$ decays $\propto 1/r^8$ and is dominated by the fluctuation-induced correlations $G_{T,P}(r)$, which both decay $\propto 1/r^6$.

References

[1] Planck Collaboration, Astron. Astrophys. 594 (2016) A1.
[2] Planck Collaboration, Astron. Astrophys. 594 (2016) A11.
[3] Planck Legacy Archive, Release PR2, 2015, http://pla.esac.esa.int/pla/.
[4] Y. Cao, Y. Zhao, X. Yue, F. Xiong, Y. Sun, X. He, L. Wang, Physica A 456 (2016) 244.
[5] A. Perera, T. Urbic, Physica A 495 (2018) 393.
[6] I. Śliwa, Physica A 498 (2018) 116.
[7] J.-L. Barrat, Physica A 504 (2018) 20.
[8] D.-P. Hao, G. Tang, Z.-P. Xun, H. Xia, K. Han, Physica A 490 (2018) 338.
[9] P.K. Shaw, D. Saha, S. Ghosh, M.S. Janaki, A.N.S. Iyengar, Physica A 469 (2017) 363.
[10] P. Mali, S. Sarkar, S. Ghosh, A. Mukhopadhyay, G. Singh, Physica A 424 (2015) 25.
[11] T. Matcharashvili, T. Chelidze, Z. Javakhishvili, N. Zhukova, Physica A 449 (2016) 136.
[12] S. Chatterjee, P. Barat, I. Mukherjee, Physica A 492 (2018) 1352.
[13] D. Subhakar, E. Chandrasekhar, Physica A 445 (2016) 57.
[14] S. Berrut, V. Pouillard, P. Richmond, B.M. Roehner, Physica A 463 (2016) 400.
[15] O. Farzadian, M.D. Niry, Physica A 450 (2016) 95.
[16] Z. Wang, Y. Yan, X. Chen, Physica A 482 (2017) 477.
[17] R. Hasan, M. Salim, Physica A 473 (2017) 620.
[18] A.S. Chakrabarti, Physica A 462 (2016) 442.
[19] S. Jiang, W. Guan, W. Zhang, X. Chen, L. Yang, Physica A 483 (2017) 227.
[20] P. Mali, S.K. Manna, A. Mukhopadhyay, P.K. Haldar, G. Singh, Physica A 493 (2018) 253.
[21] H. Xiong, P. Shang, J. Xia, J. Wang, Physica A 499 (2018) 241.
[22] R. Tomaschitz, Physica A 489 (2018) 128.
[23] R. Tomaschitz, Astropart. Phys. 84 (2016) 36.
[24] R. Tomaschitz, Physica A 483 (2017) 438.
[25] M. Born, E. Wolf, Principles of Optics, sixth ed., Pergamon, Oxford, 1980.
[26] L.D. Landau, E.M. Lifshitz, Electrodynamics of Continuous Media, second ed., Elsevier, Oxford, 1993.
[27] L.D. Landau, E.M. Lifshitz, Statistical Physics, third ed., Pergamon, Oxford, 1980.

[28] R. Tomaschitz, Mon. Not. R. Astron. Soc. 427 (2012) 1363.
[29] Healpix primer, vers. 2.15a, 2010, https://healpix.jpl.nasa.gov/pdf/intro.pdf.
[30] R. Tomaschitz, Eur. Phys. J. B 91 (2018) 115.
[31] C. Patrignani, et al., Chin. Phys. C 40 (2016) 100001.
[32] G.N. Watson, A Treatise on the Theory of Bessel Functions, Cambridge University Press, Cambridge, 1996.
[33] R.G. Newton, Scattering Theory of Waves and Particles, Springer, New York, 1982.
[34] W. Magnus, F. Oberhettinger, R.P. Soni, Formulas and Theorems for the Special Functions of Mathematical Physics, Springer, New York, 1966.
[35] F.W.J. Olver, D.W. Lozier, R.F. Boisvert, C.W. Clark, (Eds.), NIST Digital Library of Mathematical Functions, Release 1.0.18, 2018, http://dlmf.nist.gov,
[36] V. Badescu, J. Phys. III (France) 2 (1992) 1925.
[37] P.T. Landsberg, V. Badescu, Prog. Quant. Electron. 22 (1998) 211.